Ore Geology Reviews 144 (2022) 104855

Contents lists available at ScienceDirect

Ore Geology Reviews

journal homepage: www.elsevier.com/locate/oregeorev

^{40}Ar-^{39}Ar and Rb-Sr age constraints on the formation of Sukhoi-Log-style orogenic gold deposits of the Bodaibo District (Northern Transbaikalia, Russia)

Andrey V. Chugaev [a,*], Alexander E. Budyak [b], Yulia O. Larionova [a], Igor V. Chernyshev [a], Alexei V. Travin [c], Yulia I. Tarasova [b], Bulat I. Gareev [d], Georgii A. Batalin [d], Irina V. Rassokhina [a], Tatyana I. Oleinikova [a]

[a] Institute of Geology of Ore Deposits, Petrography, Mineralogy and Geochemistry, Russian Academy of Sciences, 35, Staromonetny Lane 35, Moscow 119017, Russia
[b] Vinogradov Institute of Geochemistry, Russian Academy of Science, Siberian Branch, 1A Favorsky Str, Irkutsk 664033, Russia
[c] Institute of Geology and Mineralogy, Siberian Branch of the Russian Academy of Sciences, 3, Ac. Koptyuga Ave, Novosibirsk 630090, Russia
[d] Kazan Federal University, 18, Kremlyovskaya Str, Kazan 420008, Russia

ARTICLE INFO

Keywords:
Orogenic gold deposit
Sukhoi Log
Bodaibo District
Northern Transbaikalia
Rb-Sr and ^{40}Ar-^{39}Ar dating

ABSTRACT

The Bodaibo District (the Irkutsk Region of Russia) is a world-class gold-mining subprovince comprising a total of 13 large- and medium-scale black-shale-hosted orogenic gold deposits known as the Sukhoi Log-style gold deposits (Ivanov, 2014). The gold mineralization of the Sukhoi Log-style deposits is represented by early veinlet-disseminated sulfide ores, which have the main economic significance, and late native gold-bearing quartz veins with only minor gold reserves. This paper presents the results of Rb-Sr и ^{40}Ar-^{39}Ar dating of the gold mineralization in four Sukhoi Log-style deposits: Verninsky, Golets Vysochaishy, Ozherelie, and Ikan, with the estimated gold reserves of 143, 86, 6.5, and 7.0 metric tons, respectively. The Rb-Sr and ^{40}Ar-^{39}Ar data obtained indicate the existence of two ore-forming events in the district. The early sulfide veinlet-disseminated ores formed in the Silurian (450–430 Ma) and postdate the peak of the regional metamorphism in the region.. During the middle Carboniferous (ca. 330 Ma), the rejuvenation of ore-forming processes resulted in the formation of native gold-bearing quartz veins. The constraints on the ages of gold mineralization of the Sukhoi Log-style deposits are of key importance for understanding their genesis and the features of evolution of the Bodaibo District as a gold-mining subprovince.

1. Introduction

Orogenic gold deposits associated with formation of orogenic fold belts, such as Bendigo, Kumtor, Sukhoi Log, are the major sources of gold reserves currently being mined in the world (Groves, 1993; Groves et al., 1998; Goldfarb et al., 2001, 2005, 2014; Goldfarb and Groves, 2015; Phillips, 2013). At the same time, the leading role in the global gold production belongs to the orogenic deposits, associated with carbonaceous-terrigenous black shale complexes due to their wide distribution and higher ore potential (Goldfarb et al., 2001; Large et al., 2011). Despite the long history of study of such deposits, their origin is still the subject of debate (Buryak, 1982; Kerrich and Cassidy, 1994; Groves et al., 2003; Large et al., 2007; 2011; Meffre et al., 2008; Mao et al., 2008; Frei et al., 2009; de Boorder, 2012; Groves & Santosh, 2016; Chernyshev et al., 2009; 2011, Tarasova et al., 2020). The Bodaibo District, located in the Irkutsk Region of Russia, is one of the major gold-mining provinces in the world. During the 200-year history of the prospecting, >1500 metric tons of gold have been mined here. At present, its potential resources are estimated at about 4000 metric tons, with the annual gold production over 20 metric tons (https://nedradv.ru/nedradv/ru/resources/?obj=ab05b068239ede80d3dd35cf40638bd2). For a long time, placer deposits were the main source of gold in the region. However, their depletion has led to the veinlet- disseminated and native gold-bearing quartz deposits becoming the main contributor to the regional gold production. The main resources of gold in the region are associated with orogenic deposits, localized in the Precambrian metasediments (black shale formations) of the Baikal- Patom fold belt (BPB) (Buryak & Bakulin, 1998; Large et al., 2007; Konstantinov, 2010,

* Corresponding author.
E-mail address: vassachav@mail.ru (A.V. Chugaev).

https://doi.org/10.1016/j.oregeorev.2022.104855
Received 12 August 2021; Received in revised form 2 February 2022; Accepted 22 March 2022
Available online 23 March 2022

Meffre et al., 2008; 2016). More than a dozen of large- and medium-scale gold deposits have been discovered here, including the giant Sukhoi Log deposit (ca. 1500 tons of gold, Karpenko et al., 2006). The similarity of the geological position, isotopic features and mineral composition of the deposits allowed to identify them as the Sukhoi Log-style (Buryak et al., 2002; Wood and Popov, 2006; Chugaev & Chernyshev, 2017; Tarasova et al., 2020). In the Sukhoi Log-style deposits, the mineralization occurs in the form of veinlet-disseminated sulfide stockwork and native gold-bearing quartz veins. Both ore types are often spatially associated in the deposits.

Despite extensive geological, geochemical and isotopic studies, models for ore formation in Sukhoi-Log-style gold deposits remains controversial. There are currently two main concepts involving either: magmatic or metamorphic-hydrothermal origins. According to the magmatic model, the gold mineralization is genetically linked to Paleozoic granitoid magmatism (Rundqvist et al., 1992; Laverov et al., 2000; Distler et al., 2004). The melts were emplaced into the upper crustal levels at the Late Paleozoic post-orogenic stage of the BPB evolution and were the source of hydrothermal fluids and metals, including gold (Rundqvist et al., 1992; Laverov et al., 2000, etc.). Some researchers suggested a polygenic genesis of granitoid melts, as well as participation of a mantle-derived fluid in ore-forming processes (Distler et al., 2004). The metamorphic-hydrothermal model implies a leading role of regional metamorphism in the formation of the Sukhoi Log-style deposits (Buryak and Bakulin, 1998; Large et al., 2007; Meffre et al., 2008; Belogub et al., 2014; Tarasova et al., 2020), whereby the gold and related components were extracted from the host sedimentary rocks. The ore-forming fluids were produced by dehydration and decarbonatization of host rocks during the post-peak (retrograde stage) regional metamorphism at pressures and temperatures ranging from the greenschist to amphibolite facies.

The existing disagreement about the origin of the Sukhoi Log-style deposits is largely caused by the fact that the key issue, i.e., the age of the gold mineralization, still remains unresolved. The available age constrains are limited and range widely from the Cambrian to Carboniferous. Most of data were obtained for the Sukhoi Log deposit itself (Distler et al., 2004; Wood and Popov, 2006; Laverov et al., 2007; Meffre et al., 2008; 2016; Yudovskaya et al., 2011; Yudovskaya et al., 2016; Yakubchuk et al., 2014). These data indicate the presence of two ore-forming events at the Sukhoi Log deposit. The early Paleozoic event coincides with the regional metamorphism, and the late Middle Carboniferous event coincides with the formation of the large granite intrusions in the region. Geochronological information for the other Sikhoi Log-style deposits in the district is very limited (Tarasova et al., 2021). Thus, in order to resolve the issue of the origin of gold mineralization additional gold deposits in the Bodaibo District need to be studied.

The previously published and new geochronological data will allow the correlation of the ore-forming events with the main stages of the geological evolution of the BPB. This approach provides an opportunity to test the existing genetic models for different Sukhoi Log-style deposits, including the Sukhoi Log deposit proper.

The main objective of the present study is to determine of the age of the gold mineralization for the four Sukhoi Log-style deposits of the BPB, including the Verninsky, Golets Vysochaishy, Ozherelie, and Ikan (7 tons of Au) with the estimated gold reserves of 143, 86, 6.5, and 7.0 metric tons, respectively. In terms of their geological structure and type of gold mineralization, these are the Sukhoi Log-style orogenic gold deposits (Goldfarb et al., 2001; Rusinov et al., 2008; Chugaev & Chernyshev, 2017; Tarasova et al., 2020). However, although having a lot in common, each of these deposits has a number of distinct features. Geologically, the studied deposits are confined to different stratigraphic strata of the Neoproterozoic metasedimentary sequences, including (from bottom to top) the Khomolkho, Aunakit and Dogaldyn formations. Other gold deposits within BPB are also confined to these formations. The deposits selected for the study are located in rocks of different metamorphic facies. The Ozherelye and Ikan deposits are localized in sedimentary rocks metamorphosed under the amphibolite facies, and the Verninskoye and Golets Vysochaishy deposits - in the grinschist facies.

The mineral composition of the Sukhoi Log-style ore deposits limits the choice of isotopic methods and dating approaches. We chose the Rb-Sr and ^{40}Ar-^{39}Ar methods owing to their successful application in studying the age of hydrothermal mineralization. When applied together, the complementary features of the Rb-Sr and K-Ar isotope systems allow for obtaining reliable age information permit interpretation of the data. The ^{40}Ar-^{39}Ar method was applied in this study for dating hydrothermal muscovite widespread in quartz veins and altered host rocks of the gold deposits. Muscovite is one of the most informative minerals in the ^{40}Ar-^{39}Ar isotope studies, and the approaches to obtaining and interpreting the data have been well developed over the past 40 years (Baksi, 1999; 2006; Villa, 1997; 2021). The Rb-Sr method was applied in this study for dating mineral fractions and whole-rock samples of veinlet-disseminated sulfide ores. The whole-rock Rb-Sr isotopic analysis of metasomatic rocks associated with gold mineralization has been shown to be an effective method for dating hydrothermal gold deposits (Laverov et al., 2007; Larionova et al., 2013, Zongyong et al., 2016). This approach is used with an assumption that the Rb-Sr isotope system in the host rocks has been is re-set by the hydrothermal processes that operated during ore formation. The Sukhoi Log-style veinlet-disseminated sulfide mineralization was formed at relatively high temperature (280–440 °C) and was accompanied by intense hydrothermal alteration of the host metasediments (Rusinov et al., 2008; Prokof'ev et al., 2019; Tarasova et al., 2020) causing the re-set of the Rb-Sr isotopic system. The Rb-Sr and ^{40}Ar-^{39}Ar methods have been applied for dating quartz and sulfide minerals (e.g., Kendrick et al. 2001; Qiu et al., 2002; Ivanov et al., 2015; Zhai et al., 2015). In case of the black shale hosted gold deposits, however, the low content of radiogenic ^{87}Sr and ^{40}Ar and the presence of xenogenic mineral inclusions in sulfides and secondary fluid inclusions in quartz complicate both analysis and data interpretation (e.g., Laverov et al., 2007; Chugaev et al., 2010, Tarasova et al., 2021).

2. Previous geochronological studies

There are certain difficulties that exist in dating the Sukhoi Log-type orogenic gold deposits. They are primarily causedby a limited choice of minerals suitable for isotopic dating, as well as by the limited capabilities of the available geochronological methods. Nonetheless, reliable geochronological data for the Sukhoi Log deposit do exist (Laverov et al., 2007; Meffre et al., 2008; Yudovskaya et al., 2011; Yakubchuk et al., 2014). Since the Sukhoi Log deposit is considered to be a benchmark for deposits of the Sukhoi Log-type, the previous results may provide useful information for the present isotopic study of the selected deposits.

The first direct dating of the gold mineralization in the Sukhoi Log deposit was carried out by the Rb-Sr method (Laverov et al., 2007) using two approaches. The first of them was to study samples of hydrothermally-altered metasediments containing gold veinlet-disseminated sulfide ores. The second one was to date the late quartz veins by studying the Rb-Sr isotopic system in quartz and carbonate, as well as in fluid inclusions in the quartz. The Rb-Sr isotopic data obtained for 12 whole-rock samples yielded an isochrone age of 454 ± 6 Ma and an initial $^{87}Sr/^{86}Sr = 0.7126 \pm 1$ (MSWD = 22). This age was interpreted as the age of the veinlet-disseminated sulfide mineralization. The hydrothermal quartz, fluid inclusion, and carbonate (6 samples in total) from the late quartz vein gave a regression line with a slope corresponding to an age of 326 ± 14 Ma and an initial $^{87}Sr/^{86}Sr = 0.7166 \pm 4$ (MSWD = 11).

Subsequent geochronological studies of the Sukhoi Log deposit included the U-Th-Pb isotope dating of accessory monazite (Meffre et al., 2008; Yudovskaya et al., 2011), and Re-Os isotope dating of pyrite (Yakubchuk et al., 2014). These studies did not allow for refining the age

of the Sukhoi Log gold deposit, however.

Meffre et al. (2008) studied U-Pb isotope system in monazite from the black shales of Khomolho Formation, hosting the Sukhoi Log deposit, using laser ablation inductively coupled plasma mass spectrometry (LA-ICP-MS). Cores of large monazite crystals were dated at 573 ± 12 Ma, whereas rims of some monazite grains had relatively younger ages of 516 ± 10 Ma, suggesting later peak metamorphism and deformation of the Neoproterozoic sedimentary rocks of the Bodaibo District. Finally, a small population of monazite crystals was dated at 374 ± 20 Ma and 288 ± 22 Ma reflecting the late fluid induced processes in the Sukhoi Log deposit.

Yudovskaya et al. (2011) studied monazite from ore-bearing rocks by the U-Pb-Th SHRIMP technique. They distinguished two generations of the mineral. Late monazite was found only in veinlet-disseminated sulfide ores as overgrowths, rims and blocks in larger aggregates of early monazite. The discordant ages calculated from the $^{206}Pb/^{238}U$ and $^{208}Pb/^{232}Th$ data t ranged from 739 to 365 Ma for both early and late monazite. The apparent U-Pb ages of the late monazite ranged from 486 ± 18 to 439 ± 17 Ma and reflected the time of the veinlet-disseminated sulfide ore formation.

The Re-Os isotope dating (Yakubchuk et al., 2014) of the Sukhoi Log deposit was carried out on five samples of pyrite separated from the veinlet-disseminated sulfide mineralization. The samples have high content of common Os, relatively low Re and, accordingly, low $^{187}Os/^{188}Os$ ratios ranging from 0.992 to 1.283. Large scatter of the data on the Re-Os diagram (MSWD ca. 500), however, allowed for only a general age approximation as Paleozoic.

Recently, Tarasova et al. (2021) carried out a ^{40}Ar-^{39}Ar study of two pyrite samples from the veinlet-disseminated sulfide ores of the Golets Vysochaishy gold deposit. One of the samples analyzed showed a saddle-shaped spectrum that yielded a plateau-like age of 437 ± 62 Ma for the middle- and partly the high-temperature steps. In the second sample, ^{40}Ar-^{39}Ar spectrum had a descending, staircase-type of age spectrum. It yielded a reliable plateau age of 331 ± 9 Ma (Tarasova et al., 2021).

The observed available isotope data for the Sukhoi Log-type deposits reviewed above cover the period from the Cambrian to the Carboniferous-Permian boundary, implying the existence of multistage ore-forming process in the Bodaibo District. Although these age determinations do not coincide within their uncertainties, the results may suggest 1) Early Paleozoic (Late Cambrian to Silurian) age of the early veinlet-disseminated sulfide mineralization and its temporal relation to the regional metamorphism, and 2) Late Paleozoic (Late Devonian to Carboniferous) age of the late gold-bearing quartz veins.

2.1. Geology of the Bodaibo gold district

The gold deposits selected for the geochronological study are located in the Bodaibo gold District within the Bodaibo synclinorium, one of the largest tectonic structures in the Baikal-Patom fold belt, bordering the Siberian Craton in the south (Gusev and Khain, 1995; Nemerov et al., 2010; Gladkochub et al., 2013) (Fig. 1). The Baikal-Patom fold belt in the south is bordered, in turn, by the extensive Central Asian orogenic belt (CAOB) (Zonenshain et al., 1990; Yarmolyuk et al., 2012; Kröner et al., 2014; Safonova et al., 2017).

The Bodaibo synclinorium is comprised of a thick (up to 15 km) Neoproterozoic metasedimentary sequence (Fig. 2). Detailed petrographic, lithological and geochemical characteristics of the metasediments are given in Zhuravleva et al. (1969), L'vova (1969), Korikovsky and Fedorovsky (1980), Ivanov et al. (1995), Pokrovsky et al. (2006; 2010), Nemerov et al. (2010), Chumakov et al. (2013), Budyak et al. (2016), Chugaev et al. (2017; 2018). A distinct feature of the Neoproterozoic metasedimentary sequence is a large abundance of carbonaceous (C content of up to 10 wt%) rocks (black shales, siltstones, sandstones) that host the gold mineralization in the BPB (Buryak & Bakulin, 1998). The Neoproterozoic metasedimentary sequences of the BPB are traditionally subdivided into the Patom complex, unconformably overlying the basalts of the Medvezhevsky Formation, and the Yudoma Group, conformably overlying the Patom complex (Nemerov et al., 2010; Chumakov et al., 2013). The Bodaibo synclinorium has a complex folded structure, that was formed during several episodes of ductile deformation of the Ediacaran to the Middle Cambrian sedimentary units (Buryak, 1982; Ivanov et al., 1995; Chumakov, 2016).

Deposition of the sedimentary rocks of the Bodaibo synclinorium took place during the Tonian to Ediacaran periods in deferent tectonic settings. In the early period (750–635 Ma), the sediments formed in an open marine basin to a passive-margin setting of the Siberian Craton, and then sedimentation occurred in a foreland-type basin setting (600–540 Ma) (e.g.,Gusev and Khain, 1995; Kuz'min et al., 2006; Bogdanova et al., 2009; Nemerov et al., 2010; Gladkochub et al., 2013; Chumakov et al., 2013; Powerman et al., 2015; Pokrovsky & Bujakaite, 2015; Chugaev et al., 2018; Budyak et al., 2019).

The Neoproterozoic sediments underwent polyphase metamorphism. In the central part of the Bodaibo synclinorium, the rocks are metamorphosed under the low-temperature greenschist facies. Areas of the higher metamorphic grades (epidote–amphibolite and amphibolite) occur at the periphery of the synclinorium and are confined to the areas in close proximity to the Paleozoic granitoid intrusions. Most researchers assume the Cambrian-Silurian age of the regional

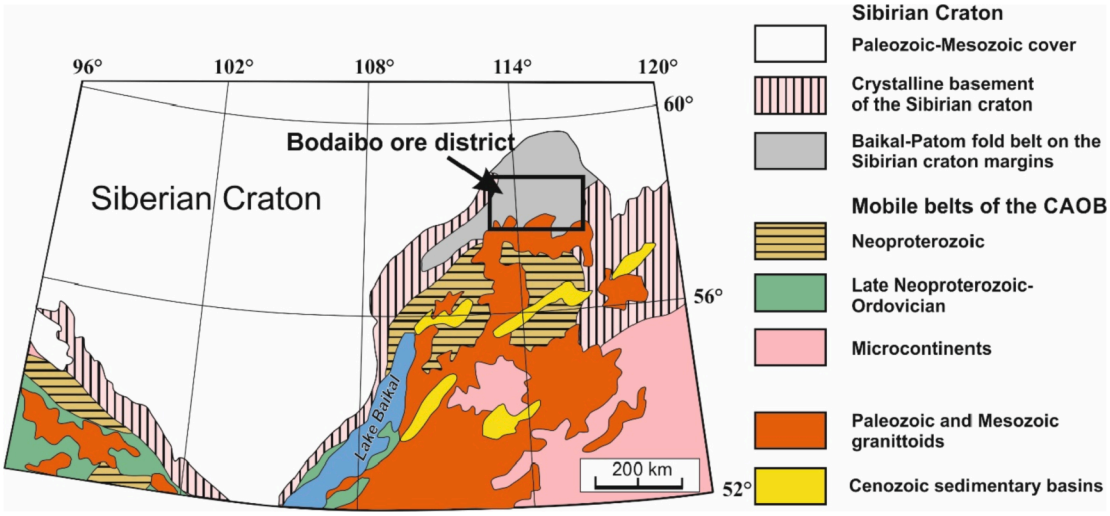

Fig. 1. Geological sketch map of the northeastern part of the Central Asian orogenic belt (CAOB) (modified after Kröner et al., 2014).

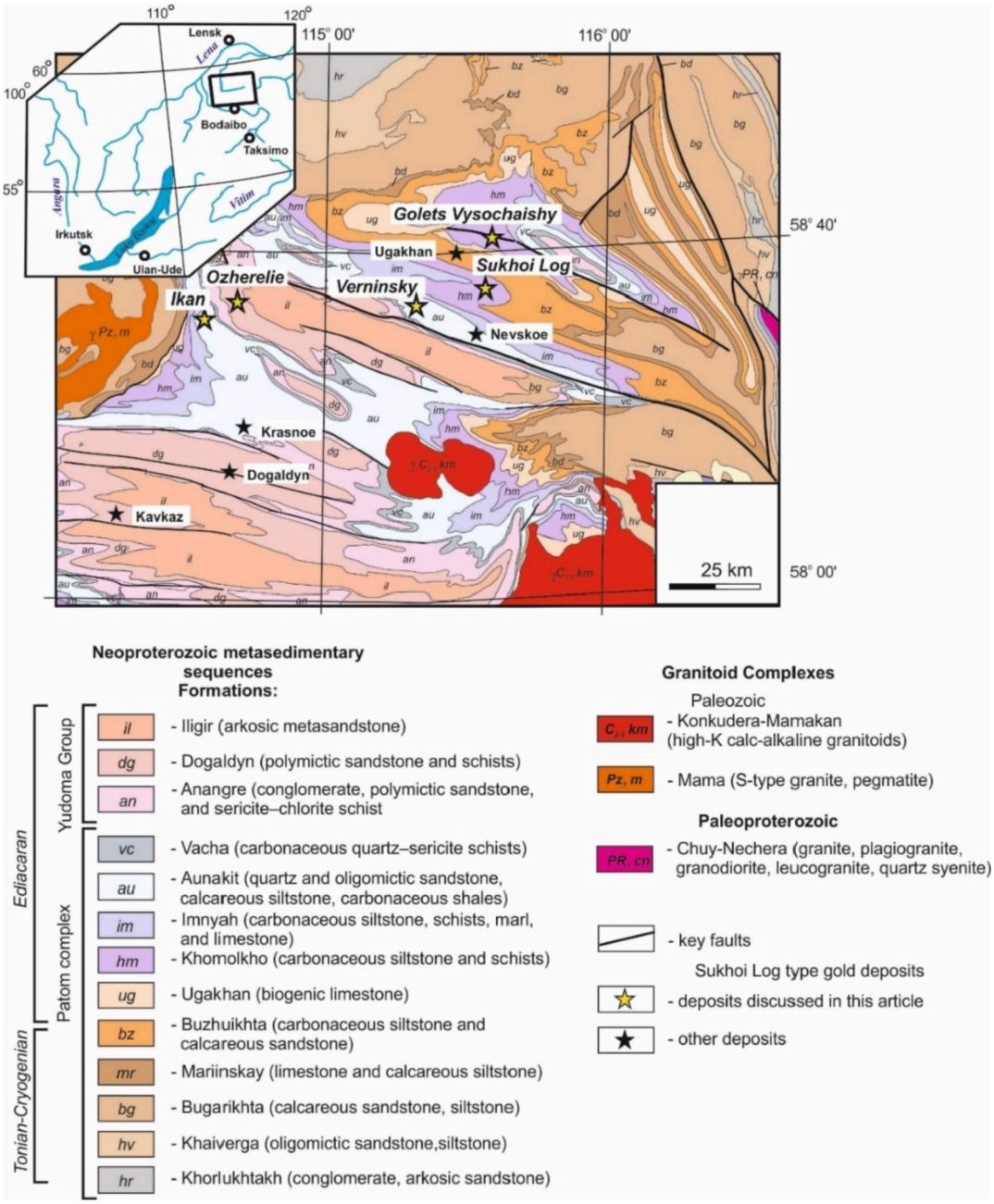

Fig. 2. Geological sketch map of the Bodaibo District (Baikal-Patom belt) and the location of the Sukhoi Log-type gold deposits (modified after Tarasova et al., 2020).

metamorphism (Buryak, 1982; Vinogradov et al., 1996; Scott et al., 2007; Zorin et al., 2008). Besides, the results of the geochronological studies indicate that the high-temperature contact metamorphism took place also in the Late Paleozoic and was associated with the emplacement of large granite massifs of the Konkudera-Mamakan complex (Neymark et al., 1993).

In the BPB, the gold mineralization is represented by two major types: veinlet-disseminated sulfide and gold-bearing quartz vein types. In the veinlet-disseminated sulfide type mineralization, ore minerals are represented predominantly by pyrite, pyrrhotite and arsenopyrite, but their relative proportions vary from deposit to deposit. The gold-bearing quartz veins, as a rule, are spatially associated with zones of the veinlet-disseminated sulfide mineralization. In quartz veins, pyrite and pyrrhotite significantly dominate over galena, sphalerite, and native gold, with the contents of ore minerals being generally below 1% (Buryak and Bakulin, 1998; Large et al., 2007; Chugaev et al., 2014; Palenova et al., 2015; Tauson et al., 2015; Tarasova et al., 2020).

The ore-forming processes within the Bodaibo synclinorium were accompanied by hydrothermal alteration of the host rocks (mainly carbonatization and silicification). The host rock alteration occurred synchronously with the development of foliation and formation of the veinlet-disseminated sulfide mineralization. The metasomatic minerals form early paragonite-siderite + ankerite-quartz ± chlorite and late muscovite- (siderite + ankerite) -pyrite-quartz assemblages. Geothermobarometric studies of the Verninsky, Golets Vysochaishy and Sukhoi Log deposits showed that the alteration process occurred at temperatures of ca. 300–350 °C and pressures of 0.7–2.8 kbar (Rusinov et al., 2008). These estimates are consistent with the data from the study of fluid inclusions in quartz from the same deposits (Safonov et al., 2012; Prokof'ev et al., 2019).

2.2. Geology of the Verninsky, Golets Vysochaishy, Ozherelie, and Ikan deposits

The geology and mineralogy of the ores in the Verninsky, Golets Vysochaishy, Ozherelie and Ikan deposits are detailed elsewhere (e.g., Buryak, 1982; Buryak & Bakulin, 1998; Ivanov, 2008; Rusinov et al., 2008; Konstantinov, 2010; Chugaev et al., 2014; Babyak et al., 2019; Prokof'ev et al., 2019). A brief description of the deposits is given below and in Table 1.

2.2.1. Verninsky deposit

The Verninsky deposit is located in the central part of the Verninsky anticline, which is a part of the larger Verninsko-Nevsky tectonic zone of a sublatitudinal strike (Fig. 2a). Its gold reserves, according to the 2019 data (OJSC Polyus Gold), are estimated at 143 metric tons (https://polyus.com/en/operations/operating_mines/verninskoe/). The metasedimentary rocks are intensively folded. The folds are generally elongated in the sublatitudinal direction, and are cut by low-amplitude faults. Among the latter, reverse-strike-slip faults and reverse-thrust faults are widespread. The mineralization of the deposit is localized in the clastic-carbonate rocks of the Aunakit Formation (total thickness of c. 500 m), which is part of the Patom complex. The Aunakit Formation is composed of quartz and calcareous sandstones, alternating with layers of carbonaceous sericite-quartz siltstones, shales, with occasional layers of black limestone. The rocks of the Formation underwent regional greenschist facies metamorphism.

The mineralization is represented by arsenopyrite-pyrite-quartz veinlets characterized by parallel-bedded orientation and disseminated arsenopyrite and pyrite grains often rimmed by quartz (Fig. 3a, b). The veinlet-disseminated sulfide ores form three zones of a sub-latitudinal strike dipping north–north-east. One of the zones is located in the core of the fold and is not exposed, while the other two (First and Second ore bodies) are located in the hanging northern and southern limbs of the structure (Fig. 3a). The northern mineralized zone is the largest: it can be traced along the strike for ~1800 m with an average thickness of ca. 70 m. In the veinlet-disseminated sulfide ores, the content of the ore minerals usually does not exceed 3–5% by volume, with pyrite and arsenopyrite being dominant, and sphalerite, chalcopyrite, galena, fahlores, native gold, and pyrrhotite present in subordinate amounts (Fig. 4c).

The gold-bearing quartz veins are spatially associated with zones of the veinlet-disseminated sulfide mineralization, cross-cutting the latter (Fig. 3b). By their strike, the veins are subconformable to the main Verninsky-Nevsky tectonic zone. They are represented, as a rule, by individual bodies with a thickness of 0.2–0.5 m dipping to the NNE. However, at the deposit's southern flank, there is an ore zone (known as the Pervenets zone) consisting of a several spatially closely associated, steeply dipping (at 55–70°) gold-bearing quartz veins. Native gold is present in quartz as grains of up to 1–2 mm in size that are spatially closely associated with sulfide aggregates or vein selvages.

a- arsenopyrite-quartz nests and veinlets in grey carbonaceous sandstone; b- late white quartz vein with carbonates and coarse-grained pyrite cuts parallel-bedding of the sulfide-quartz veinlets; c- native gold associated with pyrite and sphalerite in veinlet-disseminated sulfide ores; d- parallel–bedded bands of disseminated coarse-grained pyrite and pyrrhotite in black siltstone (Khomolkho Formation); e- late gold-bearing white quartz vein cutting metasedimentary rocks with veinlet-disseminated sulfide mineralization; f- native gold in hydrothermal altered black shale (selvage of a late quartz vein); g- coarse-grained muscovite in a late quartz vein; h- native gold in late quartz veinlet, cutting grey sandstone; i- late brownish quartz vein with coarse-grained muscovite and chlorite cutting grey siltstone with parallel-bedded pyrrhotite veinlets. Abbreviations: Asp- arsenopyrite; Qtz- quartz; Crb-carbonate; Py- pyrite; Au- native gold; Sp-sphalerite; Po- pyrrhotite; Mu-muscovite; Chl- chlorite.

2.2.2. Golets Vysochaishy deposit

The Golets Vysochaishy deposit is located ~30 km to the northeast from the Verninsky deposit, in the Khomolkho-Iligir tectonic zone. It is confined to the eastern limbs of the asymmetric Kamensk anticlinal fold (Fig. 3b). The core of the anticline is comprised of carbonate rocks of the Ugakhan Formation. Those are conformably overlain by black shales and carbonaceous siltstones of the Khomolkho Formation that form the limbs of the folded structure.

The veinlet-disseminated sulfide ores are localized mainly in the rocks of the lower part of the Khomolkho Formation. The gold-sulfide mineralization forms a zone of sub-latitudinal strike and gentle dip (Fig. 3b). It can be traced along the strike for up to 2 km, and for 1 km along the dip, with an average thickness of ~60 m. Two ore bodies were identified, named the Western and Eastern bodies. Both ore bodies are ~600 m long, having the dips and strikes similar to those of the main ore

Table 1
Geological and mineralogical features of the Sukhoi Log-style deposits from the Bodaibo District (Northern Transbaikalia, Russia).

Deposit	Host Formation	Ore styles	Ore minerals major/minor	Gold fineness	P-T conditionsveinlet-disseminated sulfide mineralization (V-D) /quartz vein (Q-V)	Hydrothermal alteration of host rocks (secondary assemblage)	Resource (Au, metric tons)
Sukhoi Log	Khomolkho	veinlet-disseminated mineralization + quartz vein	Py, Po, Asp, Au/ Chp, Sp, Gn, Pln	750 – 950	(V-D) T = 210–380 °C; P = 1.3–2.3 kb/(Q-V) T = 190–280 °C; P = 0.27 – 0.5 kb	quartz + muscovite + carbonate + chlorite	> 1500
Verninsky	Aunakit	veinlet-disseminated mineralization + quartz vein	Py, Asp, Po, Au/ Chp, Sp, Gn, Pln	920 – 970	(V-D) T = 252–356 °C, P = 1.6–2.1 kb	same	143
Golets Vysochaishy	Khomolkho	veinlet-disseminated mineralization + quartz vein	Py, Po, Au/ Asp, Chp, Sp, Gn, Pln	750 – 950	(V-D) T = 360–440 °C; P = 2.8 kb/ (Q-V) T = 200–360 °C; P = 0.2 – 0.5 kb	same	85.6
Ozherelie	Dogaldyn	quartz vein	Au, Py, Po/ Asp, Il, Chp, Bst	940 – 970	(Q-V) T = 280–325 °C; P = 1.8 – 2.3 kb	same	6.5
Ikan	Aunakit	veinlet-disseminated mineralization + quartz vein	Py, Po, Il, Mt, Au/ Asp, Chp, Sp, Gn	950 – 990	No data	same	7.0

Abbreviations: Py- pyrite; Po- pyrrhotite; Asp- arsenopyrite; Chp – chalcopyrite; Sp-sphalerite; Gn – galena; Au- native gold; Pln – pentlandite; Bst – bismuthinite; Il – ilmenite; Mt - magnetite. The table summarizes data from (Buryak & Khmelevskaya, 1997; Konstantinov, 2010; Safonov et al., 2012; Ivanov, 2014; Yudovskaya et al., 2016; Prokof'ev et al., 2019; Babyak et al., 2019; Tarasova et al., 2020).

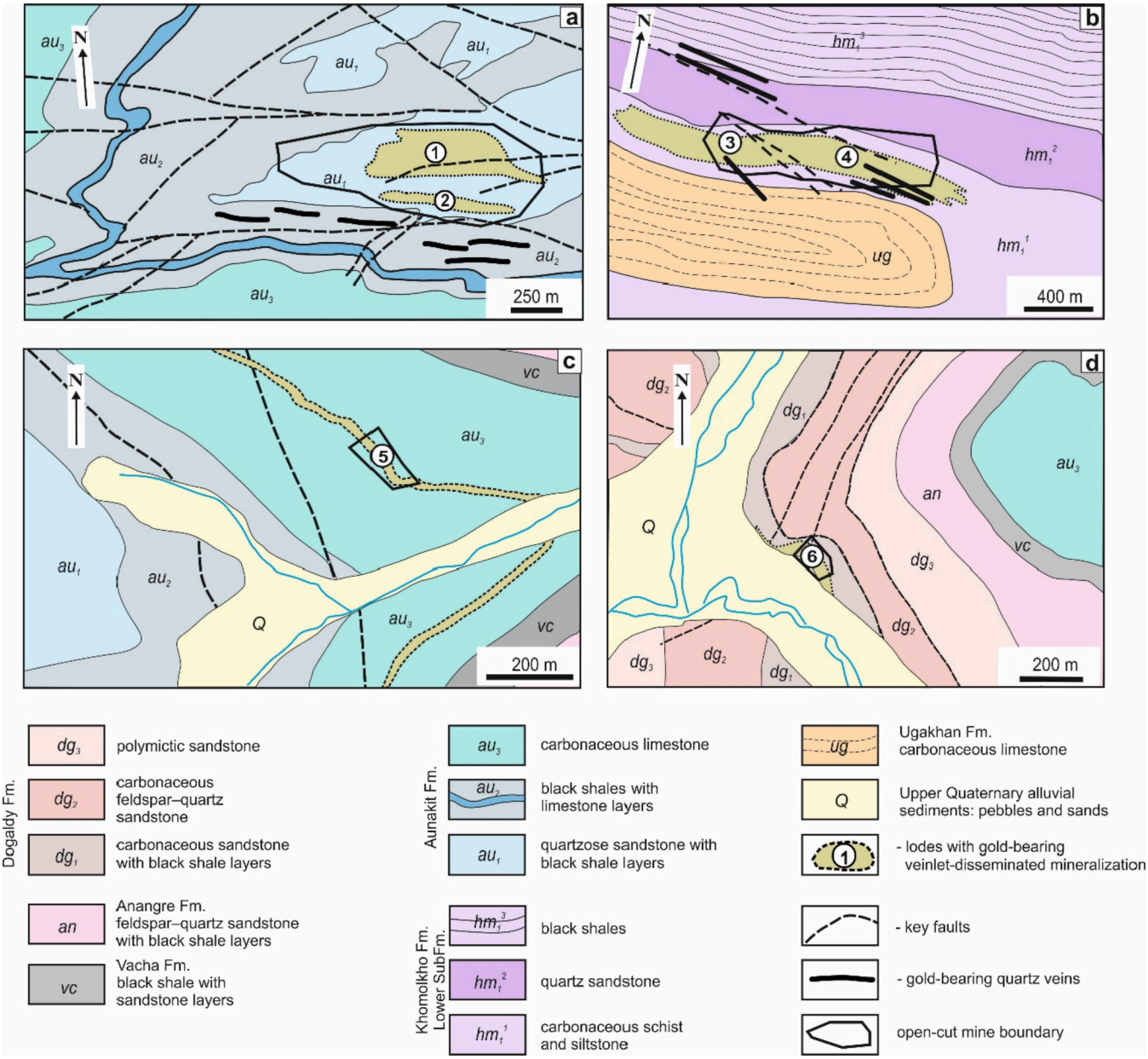

Fig. 3. Geological sketch maps of the gold deposits from this study: (a) Verninsky, (b) Golets Vysochaishy, (c) Ikan, and (d) Ozherelie (modified after Buryak and Bakulin, 1998; Ivanov, 2008; Rusinov et al., 2008; Konstantinov, 2010; Chugaev et al., 2014; Babyak et al., 2019). Ore bodies (1–6): Verninsky – 1- First, 2- Second; Golets Vysochaishy – 3- Western, 4- Eastern; Ikan – 5- Main; Ozherelie – 6- Zone No. 1.

zone of the deposit.

The gold-sulfide mineralization is composed of thin quartz-sulfide veinlets and disseminated sulfide grains. The latter type is represented by isolated euhedral (cubic or tabular forms) pyrite crystals, as well as lenticular pyrrhotite grains (Fig. 4d). The sulfide content in the veinlet-disseminated ore ranges between 2 and 3.5%. The main ore minerals are pyrite and pyrrhotite, with sphalerite, galena, chalcopyrite, and marcasite present in subordinate amounts. Gold in the deposit is distributed unevenly. It is present as native gold (grain size typically ≤500 μm) in pyrite and pyrrhotite within the quartz-sulfide veinlets.

There are also gold-bearing veins at the deposit. They occur as individual steeply dipping bodies of northwestern strike with a thickness of 0.1–0.4 m. The veins contain small amount (≤1%) of ore minerals, including pyrite, pyrrhotite, galena, sphalerite, and native gold (Fig. 4d, f).

2.2.3. *Ozherelie deposit*

The Ozherelie deposit is located ~40 km to the west from the Verninsky deposit. It is confined to the Dogaldyn anticline, which form the northeastern limb of the Marakan-Tunguska syncline. The ore bodies, whose position is controlled by the NW-striking thrusts, are represented by stockwork zones with quartz veins and veinlets of irregular thickness and length (Fig. 3c, Fig. 4g, h). The host rocks are sandstones, siltstones, and carbonaceous shales of the Dogaldyn Formation of the Yudoma Group. They underwent amphibolite facies metamorphism, which resulted in formation of biotite, garnet, amphibole, and kyanite in the rocks. In the ore zone, the host rocks are altered. The alteration assemblages are comprised of quartz, Fe-Mg-carbonates, muscovite, tourmaline, and pyrite. The largest ore body is the Ore Zone No. 1, which is ~700 m long. The sulfide content in quartz veins and veinlets does not exceed 1%. Ore minerals are represented by pyrite, pyrrhotite, chalcopyrite, and arsenopyrite. Native gold is often associated with pyrrhotite

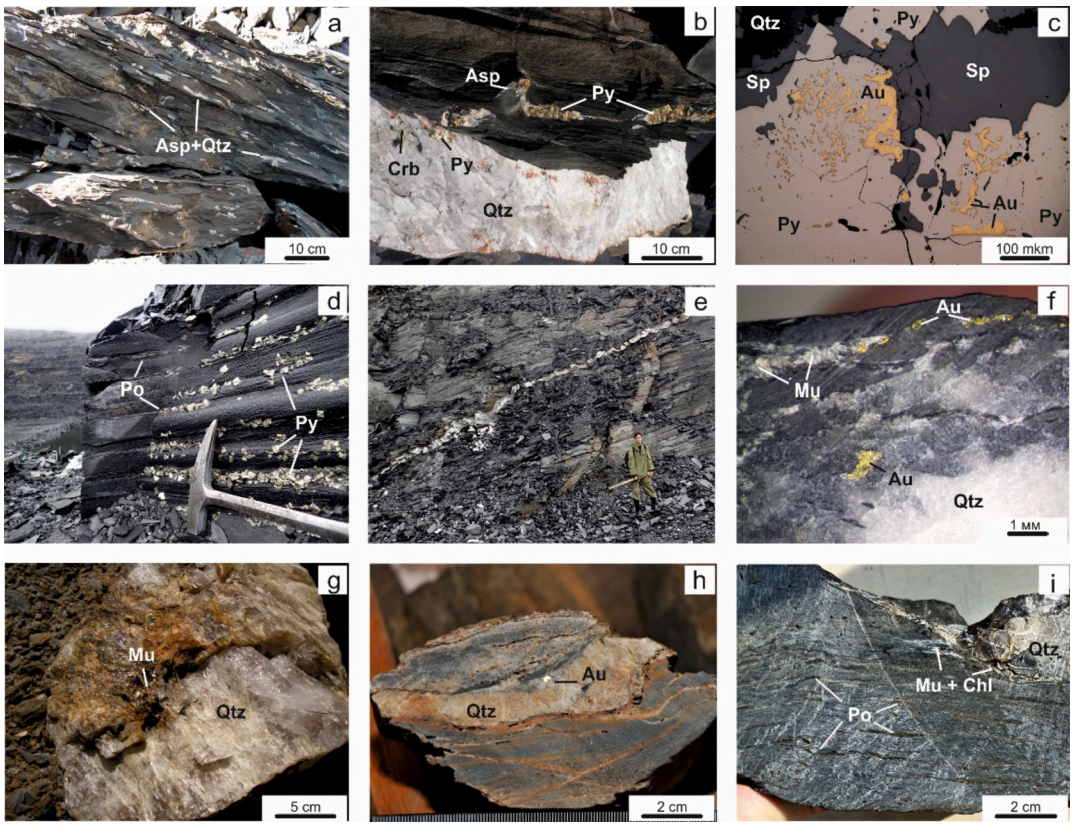

Fig. 4. Mineralogical and structural features of the veinlet-disseminated sulfide mineralization and late quartz vein from the Sukhoi Log-style deposits: (a-c) Verninsky, (d-f) Golets Vysochaishy, (g-h) Ozherelie, and (i) Ikan.

or pyrite and occurs as isolated (up to 1.5 mm in size) grains (Fig. 3h). Quartz dominates over other gangue minerals - muscovite and ankerite.

2.2.4. Ikan deposit

The Ikan deposit is located 20 km SW from the Ozherelie deposit. The deposit occurs in the north-eastern limb of the Vacha anticline, which forms SW limb of the Marakan-Tunguska syncline. An extended (ca. 4 km) gold-bearing zone of NW strike and gentle dip has been identified within the deposit (Fig. 3e). It is hosted by the Aunakit Formation metasediments of the Yudoma Group. These are dominated by carbonaceous and non-carbonaceous quartz sandstone interbedded with black shales containing biotite, muscovite, and garnet. The host rocks within the ore body are intensely foliated and altered, resulting in the development of muscovite, chlorite and quartz, as well as sulfide mineralization. Ore is represented by disseminated pyrrhotite and pyrite grains and thin (<1 cm) quartz-sulfide veinlets (Fig. 4i). The minor ore minerals include arsenopyrite, chalcopyrite, sphalerite, and galena. Gold forms small (<70 μm) grains associated with pyrrhotite. The veinlet-disseminated sulfide ores are cut by quartz veins containing pyrrhotite and pyrite. Among the gangue minerals, in addition to quartz, the veins contain small amounts of carbonates and chlorite, which, as a rule, are confined to the selvages of the veins.

3. Sampling

The geochronological studies were carried out using ore-bearing and barren rock samples collected by the authors during fieldwork at the Verninsky, Golets Vysochaishy, Ozherelie and Ikan deposits in 2003, 2010, 2018 and 2019. The ^{40}Ar-^{39}Ar and Rb-Sr isotope analyses were preceded by mineralogical and geochemical studies, allowing to select 34 samples most suitable for the dating. They represent the main types of the gold mineralization (Fig. 5).

From the Verninsky deposit, six samples of veinlet-disseminated sulfide ores, hosted by carbonaceous fine-grained quartz sandstone, quartz-sericite-carbonate siltstones, and shales were studied. The mineralization in the samples is represented by up to 2 cm in size, euhedral arsenopyrite grains rimmed by quartz and quartz-sulfide (arsenopyrite + pyrite) veinlets, surrounded by fine disseminated pyrite grains (≤1 mm in size) (Fig. 5a, b, h).

From the veinlet-disseminated mineralization of the Golets Vysochaishy deposit, 13 samples for geochronological study were selected. The ore minerals are mainly represented by disseminated pyrrhotite and pyrite. In carbonaceous quartz-sericite-chlorite schists and quartz sandstones they form separate lenses, sulfide and thin quartz-sulfide veinlets (Fig. 4c-e, i-j). The late gold-bearing quartz veins were dated using 5 hydrothermally altered rocks sampled along the contacts of quartz veins. The samples contain lenticular aggregates (up to 2 mm in size) of secondary sericite oriented along the layering of the host rocks (Fig. 5e, f).

a-b- disseminated coarse euhedral arsenopyrite rimmed by quartz in carbonaceous quartz-carbonate-sericite siltstone (a- V-5/10, b- V-2/10); c- isolated parallel-bedded pyrrhotite grains in grey sandstone (V-03-14); d, e- parallel-bedded lenticular aggregates and veinlets of pyrrhotite associated with euhedral to subhedral coarse-grained pyrite in carbonaceous quartz-sericite-chlorite shale (V-03-24); h- coarse-grained arsenopyrite rimmed by fine-grained quartz in carbonaceous quartz-carbonate-sericite siltstone (V-7/10); i- metamorphic pyrite replaced by post-metamorphic marcasite (Vch-13/10); k- sulfide-quartz veinlet in carbonaceous shale (Vch-15-10); l- deformed coarse-grained pyrrhotite in quartz-sericite sandstone (Ik-70); m- post-metamorphic quartz and chlorite replacing metamorphic garnet in quartz-sericite-chlorite siltstone (Ik-72). See Fig. 4 for the abbreviations.

At the Ozherelie deposit 5 samples with muscovite and carbonate were sampled from contact of a gold-bearing quartz vein with

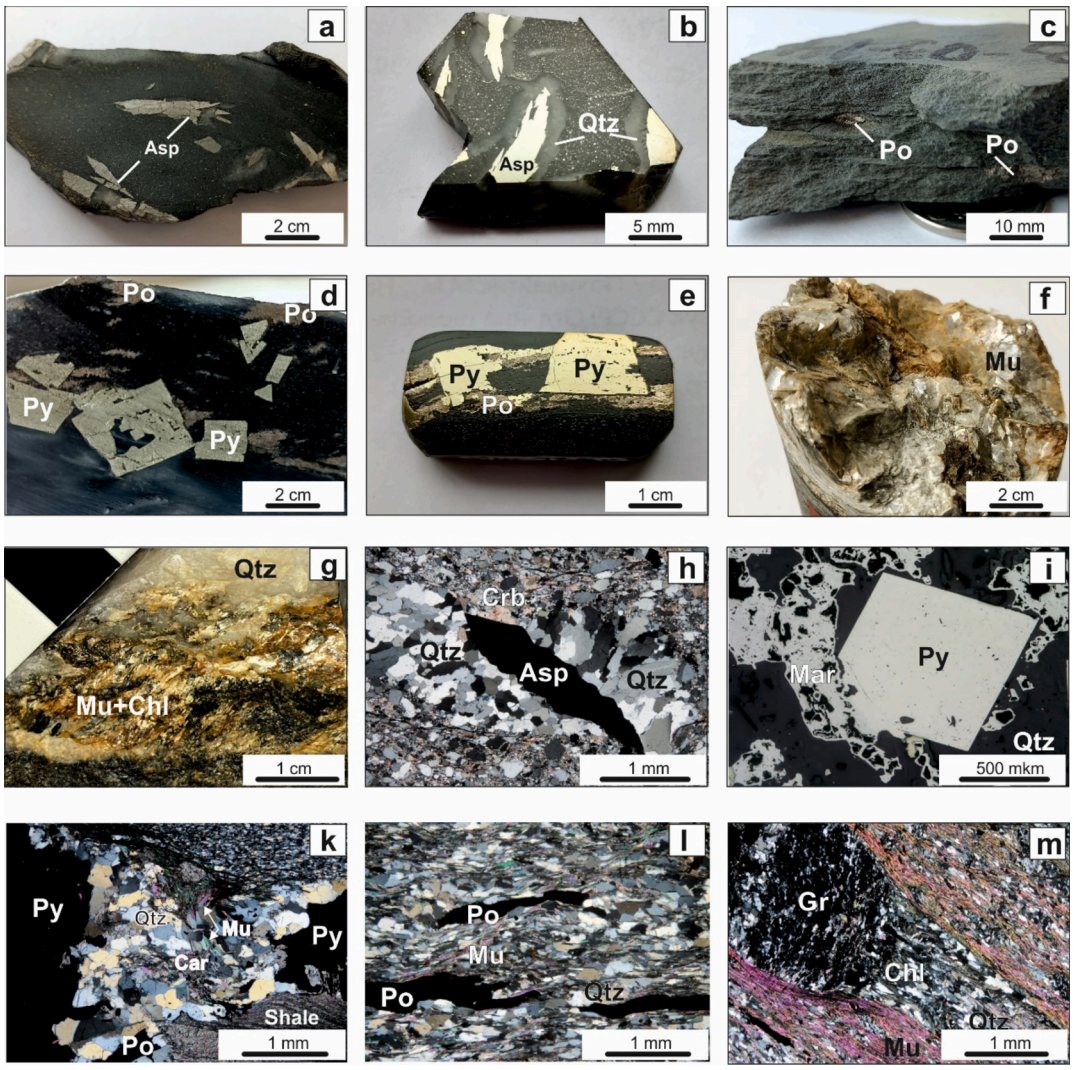

Fig. 5. Relationships between the ore and gangue minerals in the veinlet-disseminated sulfide ores and quartz veins from the studied gold deposits: a-g – hand specimens, i- reflected light, other- transmitted light, crossed polars. (a, b, h) Verninsky; (c-e, i, k) Golets Vysochaishy; (f) Ozherelie; (g, l, m) Ikan.

carbonaceous sandstones (Fig. 5f). As a rule, these are coarse-grained aggregates of muscovite, which, together with carbonate and quartz, form nests or veinlets in silicified sandstones. The observed textural relationships indicate that the studied minerals have formed simultaneously with gold-bearing quartz during a single hydrothermal process.

In the Ikan deposit, the Rb-Sr study was carried out for both types of gold-bearing mineralization, i.e., the veinlet-disseminated sulfide ores and quartz veins (Fig. 5g, l, m). From the veinlet-disseminated sulfide ores, two samples of quartz-sericite-chlorite sandstones, containing deformed lenticular pyrrhotite grains, were sampled. One of the samples (IK-72) contains rounded garnet grains, replaced by chlorite and quartz (Fig. 4i, Fig. 5l, m). The gold-bearing quartz veins are represented by two samples, containing rare disseminated pyrrhotite and pyrite. Coarse-grained chlorite and muscovite aggregates are also present, forming thick (up to 1 cm) rims along the selvages of the quartz veins (Fig. 5g). For the purposes of dating, chlorite and muscovite were separated from the samples.

In addition to the samples collected within the four gold deposits, one sample was collected from an outcrop of the Silurian muscovite-garnet granites of the Mama complex, located near the Ozherelie and Ikan deposits. The granites are composed of coarse-grained K-feldspar, quartz, plagioclase, muscovite, and garnet.

Additional information about the studied samples is given in Table 2.

4. Sample processing and analytical procedures

4.1. Sample processing

After petrographic investigation, the selected samples were hand-crushed using a carbon steel mortar and pestle down to 0.5–0.25 mm grain size. The crushed material was divided into three aliquots. One aliquot was used to separate the muscovite and chlorite fractions using the standard techniques of magnetic and heavy liquid separation, with final mineral hand-picking under binocular microscope. For XRF, ICP-MS and Rb-Sr whole-rock analyses, the second aliquot hand-pulverized down to <40 μm grain size using an agate mortar and pestle. For Rb-Sr analysis, the third aliquot was hand-crushed using a carbon steel mortar and pestle down to <0.1 mm. The crush loaded into a quartz glass dish filled with 18.2 MΩ de-ionized water and gently stirred. After the dense fraction settled, the light, float fraction (F-fraction), enriched in sericite, was decanted into a Teflon test tube and dried down. A small amount of the heavy fraction (H-fraction) was also transferred to another Teflon tube and dried down.

4.2. Chemical and XRD analysis techniques

The major element abundances were determined by X-ray fluorescence analysis at IGEM RAS using a PW-2400 spectrometer (Philips

Table 2
Summary of the sampling location and description for studied samples from the Verninsky, Golets Vysochaishy, Ozherelie, and Ikan deposits (coordinates are in the WGS-84 system).

Sample	Sampling location	Description
Verninsky deposit		
N 58 32,11′		
E 115 22,19′		
veinlet-disseminated sulfide mineralization		
V-2/10	First body, level 940 m, south-eastern boundary of the open-pit	2–3 cm coarse disseminated euhedral arsenopyrite rimmed by quartz in carbonaceous quartz-carbonate-sericite siltstone
V-3/10	Same	fine disseminated euhedral pyrite and coarse-grained arsenopyrite rimmed by quartz in carbonaceous sandstone
V-5/10	Same	2–3 cm coarse disseminated euhedral arsenopyrite rimmed by quartz in carbonaceous quartz-carbonate-sericite siltstone
V-7/10	Same	isolated coarse-grained arsenopyrite (up to 3 cm in size) rimmed by quartz in carbonaceous black shale
V-7/10a	Same	isolated cubic pyrite (up to 1 cm in size) rimmed by quartz in carbonaceous quartz-carbonate-sericite
V-14/10	First body, level 930 m, south boundary of the open-pit	irregular quartz-pyrite veinlet is 1 cm thick in carbonaceous sandstone
Golets Vysochaishy deposit		
N 58 44,53′		
E 115 34,37′		
veinlet-disseminated sulfide mineralization		
Vch-1/10	Western body, level 1060 m (western boundary of the open-pit)	isolated cubic grains of pyrite (up to 2 cm in size) in carbonaceous quartz-sericite-chlorite shale
Vch-9/10	Same	irregular pyrite-pyrrhotite-quartz veinlet in carbonaceous quartz-sericite siltstone
Vch-13/10	Eastern body, level 1050 m (south-eastern boundary of the open-pit)	parallel-bedded pyrrhotite-pyrite veinlet in black shale
Vch-15/10	Eastern body, level 1045 m (south-eastern boundary of the open-pit)	sulfide (pyrite-pyrrhotite)-quartz veinlet in carbonaceous shale
Vch-17/10	Eastern body, level 1045 m (north boundary of the open-cut mine)	same
Vch-19/10	Eastern body, level 1040 m (center of the open-pit)	2 cm-thick sulfide veinlet containing pyrite (~30%) and pyrrhotite (~60%) and quartz (~10%) in carbonaceous shale
Vch-22/10	Eastern body, level 1045 m (central part of the open-pit)	same
V-03-14	Eastern body, level 1140 m (eastern boundary of the open-pit)	isolated parallel-bedded pyrrhotite grains (up to 1 cm in size) in grey sandstone
V-03-22	Eastern body, level 1100 m (eastern boundary of the open-pit)	isolated coarse-grained euhedral pyrite (up to 1 cm in size) and parallel-bedded fine disseminated pyrrhotite in carbonaceous silstone
V-03-23	Eastern body, level 1080 m (eastern boundary of the open-pit)	isolated cubic pyrite from 0.5 to 2 cm and parallel-bedded lenticular grains of pyrrhotite in carbonaceous shale
V-03-24	Eastern body, level 1060 m (eastern boundary of the open-pit)	parallel-bedded lenticular aggregates and thin veinlets of pyrrhotite associated with euhedral to subhedral coarse-grained pyrite in carbonaceous quartz-sericite-chlorite shale
V-03-25	Eastern body, level 1040 m (eastern boundary of the open-pit)	quartz-pyrrhotite-pyrite veinlet in carbonaceous quartz-sericite-chlorite shale
V-03-26	Eastern body, level 1020 m (eastern boundary of the open-pit)	isolated parallel-bedded lenticular grains (up to 0.5 cm in size) of pyrrhotite and coarse euhedral pyrite in black sandstone
Late gold-bearing quartz vein mineralization		
Vys-2/19	Eastern body, level 1020 m (central part of the open-pit, drill hole GS-24/14, 214.4–214.5 m)	isolated parallel-bedded fine-grained muscovite aggregates (up to 4 mm in size) and thin (1–2 mm) irregular muscovite-quartz veinlets in altered black shale at contact with quartz vein with base metal mineralization
Vys-3/19	Eastern body, level 1020 m (central part of the open-pit, drill hole GS-24/14, 214.6–214.7 m)	same
Vys-4/19	Eastern body, level 1020 m (central part of the open-pit, drill hole GS-24/14, 214.8–214.9 m)	same
GV-3/18	Eastern body, level 1020 m (south-western boundary of the open-pit)	quartz vein with peripheral base metal mineralization and coarse-grained muscovite aggregates cuts metasedimentary rocks.
GV-5/18	same	same
Ozherelie deposit		
N 58 37,91′		
E 114 43,76′		
Late gold-bearing quartz vein mineralization		
OZh-1/10	Lode No. 1, level 810 m, western boundary of the open-cut mine	muscovite-quartz veinlet with carbonate at selvage of the Lode No. 1
OZh-1/18	Same	Same
OZh-2/18	Same	Same
OZh-3/18	Same	Same
OZh-4/18	Same	Same
Ikan deposit		
N 58 33,51′		
E 114 36,06′		
veinlet-disseminated sulfide mineralization		
Ik-70	Main body, level 950 m, central part of the open-pit	deformed coarse-grained pyrrhotite in laminated quartz-sericite sandstone
Ik-72	Same	pyrrhotite veinlet (up to 1 cm in thickness) in quartz-sericite-chlorite siltstone
Late gold-bearing quartz vein mineralization		
Ik-3/18	Same	quartz vein (up to 10 cm in thickness) with coarse-grained sulfide (pyrrhotite + pyrite) aggregates in grey sandstone. Coarse-grained (up to 3–4 mm in size) chlorite + muscovite aggregates are at selvage of the vein
Ik-7/18	Same	Same
Mama complex	N 58 36.28′E 114 26.66′	
Granma-1/18	Outcrop of garnet-muscovite granite	K-feldspar (45%), quartz (20%), plagioclase (15%), muscovite (15%), and garnet (5%).

Analytical B.V.). The trace elements (including Rb and Sr) were analysed by ICP-MS in the laboratory of isotopic and elemental analysis of KFU. For the ICP-MS analysis, chemical digestion of the whole-rock samples was carried out in an inorganic acid mixture by microwave digestion technique of Bettinelli et al. (2000). Indium was added to sample

solutions as an internal standards to monitor the signal drift during the analysis. The sample solutions were analysed using a ThermoFisher Scientific iCAP SQ ICP-MS instrument. The detection limits were 0.03–0.05 μg/g for Co; 0.1–0.3 μg/g for Cr, Ni, Y; Zr; Cu, and As, and 0.5–0.6 μg/g for Zn.

The mineral fractions enriched in muscovite and chlorite were studied by XRD analysis at the Institute of Geology and Chemistry of the Siberian Branch of the Russian Academy of Sciences (Irkutsk). The analysis was carried out using a D8 ADVANCE Bruker powder diffractometer equipped with a scintillation detector and a Göbel mirror. In a stepwise registration mode, when the diffraction angles 2θ range from 3 to 70°, a CuKα irradiation source was used. The data were processed using the DIFFRACplu software package, the PDF-2 powder diffractometry database (ICDD, 2007), and the EVA software. A relative percentage of phases was determined using a full-profile Rietveld method analysis with the TOPAS 4 program.

4.3. ^{40}Ar-^{39}Ar dating

The ^{40}Ar-^{39}Ar dating of muscovite was carried out by step-heating technique (Travin et al. 2009; Novikova et al., 2016; Yudin et al., 2021). For the $^{40}Ar/^{39}Ar$-analysis, 0.25–0.50 mm fractions of muscovite grains were washed in de-ionized water and then dried at 70C. The samples were wrapped in aluminum foil and stacked in quartz vials with the biotite standard MSA-11. The MSA-11 standard was calibrated (apparent age = 311.0 ± 1.5 Ma, Yudin et al., 2021) against the international standard samples Bern 4 m (muscovite, 18.5 Ma), LP-6 (biotite, 128.1 Ma), and MMhb-1 (hornblende, 514.5 Ma) (Baksi et al., 1996). The quartz vials with the samples and the MSA-11 standard were degassed at 150C, pumped out, sealed and placed into an aluminum can 5 cm in diameter. The can was filled with boron carbide for shielding slow neutrons, sealed, and irradiated at the research reactor of the Tomsk Technological University. During the irradiation, the aluminum can was continuously cooled with water, which allowed to maintain the temperature below 100C regardless of the duration of irradiation. The pumping out the quartz vials, along with the controlled thermal regime, excluded the possibility of sample contamination by atmospheric ^{40}Ar. The neutron flux gradient did not exceed 0.5% of the sample size. Using the measured positions of the MSA-11 packets in the quartz vial, the *J* value was calculated for each sample by regressing a second order polynomial equation ($J(x) = ax^2 + bx + c$). The error on individual *J-factor* values is conservatively estimated at ± 1σ.

The irradiated samples were loaded into nickel foil packets for step-heating experiments. Each sample was degassed overnight (10–12 h) at 300C to reduce atmospheric argon levels prior to analysis. Step-heating was carried out in a quartz reactor with an external furnace over a 500–1500C range of temperatures. Heating to the desired step temperature was achieved over 5 min, with the temperature being kept constant at each step for 10 min. Flux monitors (MSA-11) were heated up 1200C and then fused for 10 min. The extracted gas was purified by four ZrAl-SAES getters for 10 min. System blanks at 1200C (10 min) determined prior to each sample degassing step were typically below ~ 3×10^{-10} for ^{40}Ar, ~0.02×10^{-10} for ^{39}Ar, ~0.2×10^{-10} for ^{38}Ar, ~0.01×10^{-10} for ^{37}Ar, and ~0.09×10^{-10} cm^3 STP for ^{36}Ar. The $^{40}Ar/^{36}Ar$ ratio of the blanks was close to the atmospheric ratios. The blank was subtracted from the data for the samples. Special attention was paid to monitoring the mass discrimination factor by measuring purified atmospheric argon before each measurement. The mean $^{40}Ar/^{36}Ar$ ratio was 298 ± 2. Mass-bias was corrected for assuming linear mass-dependent fractionation and using an atmospheric $^{40}Ar/^{36}Ar = 295.5$ (Steiger and Jäger, 1977).

The Ar isotope composition was measured on a single-collector Micromass Noble gas 5400 mass spectrometer, equipped with a Faraday collector and a 10^{11} Ω resistor. Isotope ratios were extrapolated to zero time by the linear regression from sixteen cycle measurements. The argon isotopic data were corrected for baselines, mass discrimination, radioactive decay of ^{37}Ar, reactor-induced interference reactions and atmospheric argon contamination. The baseline values were measured at the beginning of each cycle and the corresponding corrections were applied automatically. For mass-discrimination correction, the weighted mean of $^{40}Ar/^{36}Ar$ values for atmospheric argon measured during sample analyses was used; Ar isotope intensities were multiplied by a coefficient characterizing linear dependence of mass spectrometer sensitivity for Ar isotope masses. Correction factors for Ca- and K-derived interfering isotopes were $(^{39}Ar/^{37}Ar)_{Ca}$ = 0.001279 ± 0.000061, $(^{36}Ar/^{37}Ar)_{Ca}$ = 0.000613 ± 0.000084, $(^{40}Ar/^{39}Ar)_{K}$ = 0.0191 ± 0.0018. The errors on the correction factors values were estimated at ± 1σ. The intermediate plateaus in the age spectra were established via applying the criteria from Fleck et al. (1977) and Baksi (1999, 2006). More specifically, at least ≥ 50% ^{39}Ar released was assumed to be enough for three successive steps revealing concordant ages. Ages were calculated with the ^{40}K decay constant ($\lambda_{40K} = (\lambda_{\beta-} + \lambda_{ec} + \lambda_{\cdot ec}) = 5.543 \times 10^{-10}$ a^{-1}) from Steiger and Jäger (1977) and the ^{37}Ar decay constant from Faure (1986). All errors on the ages are reported at the ± 2σ level and included the analytical uncertainties of the measurements of the relative Ar isotope abundance, *J value*, correction factors for interfering nuclear reactions, and the $^{40}Ar/^{36}Ar$ ratio in the atmospheric argon. The plateau ages are inverse-variance-weighted mean of selected steps. The ^{40}Ar-^{39}Ar age spectrum and inverse isochrons were plotted ISOPLOT (Version 3.71, Ludwig, 2009). Long-term reproducibility of ^{40}Ar-^{39}Ar ages obtained for the standards is presented in Appendix A1.

4.4. Rb-Sr dating

For the Rb-Sr isotope studies, typical sample weights were 10–20 mg for the mineral separates, and 30–50 mg for the whole-rock samples. Digestion of the samples was carried out in a 3: 1 mixture of conc. HF + HNO_3 at 120–140 °C in screw-cap PFA vials. Contents of Rb and Sr were determined by the isotope dilution technique. Mixed ^{85}Rb – ^{84}Sr spike was added to the samples before digestion. Rb and Sr were separated via the conventional ion-exchange chromatography using AG50 × 8 cation exchange resin (200–400 mesh) (Larionova et al., 2013; Chugaev et al., 2017). Separation of Rb and Sr was carried out in quartz columns filled with 3 mL of resin. The total procedural blanks were 0.1 ng for Rb and 0.2 ng for Sr.

Isotopic ratios of Rb and Sr were measured on a Sector 54 mass spectrometer in static and dynamic multicollection modes, respectively (Thirlwall, 1991). Strontium isotopic data were corrected for instrumental mass fractionation using $^{86}Sr/^{88}Sr = 0.11940$ and the power law. Precision and accuracy of the results were monitored via analyses of the NIST SRM 987 Sr isotope standard. During the current analytical campaign, the measured $^{87}Sr/^{86}Sr$ ratio averaged 0.710248 ± 22 (2SD, n = 9). This result is in good agreement with the data for this standard reported by Thirlwall (1991). Long-term reproducibility of Sr isotope analysis of rock standards is presented in Appendix A1.

The Rb-Sr data were regressed using ISOPLOT (Version 3.71, Ludwig, 2009). For the Rb-Sr isochron calculations, the uncertainties of ±0.005% (2σ) for $^{87}Sr/^{86}Sr$ and ± 0.5% (2σ) for $^{87}Rb/^{86}Sr$ ratios were used as determined by the analysis of the standards. The ^{87}Rb decay constant of 1.3972 ± 0.0045 × $10^{-11}a^{-1}$ from Villa et al. (2015) has been used.

5. Results

5.1. Mineralogical characteristics of the muscovite and chlorite

In the samples studied, muscovite and chlorite together with quartz and carbonate, compose the mineral association related to the hydrothermal processes of ore formation. The relative proportion of the minerals varies considerably from sample to sample. Optical microscopy of the samples did not reveal any signs of later superimposed processes,

except in the samples of quartz veins from the Ozherelie deposit which contain hydrothermal carbonate partially replaced by iron hydroxide.

According to the X-ray diffraction results, the muscovite from the separates obtained for the ^{40}Ar-^{39}Ar and Rb-Sr dating is of polytype 2 M1. The separates contained some carbonate (<5 vol%, in the Verninsky, Ozherelie, and Golets Vysochaishy deposits) and chlorite (<10 vol% in the Ikan deposit). The chlorite from the Ikan deposit obtained for the Rb-Sr study and identified as clinochlore was 95–99 vol% pure and contained some muscovite and quartz.

5.2. Major and trace element abundances

Major and trace element abundances in the whole-rock samples are presented in the Supplementary Appendix A1. Major oxide concentrations vary significantly in the ore-bearing rocks of the Verninsky, Golets Vysochaishy, and Ikan deposits, with most variability observed for the major ore mineral components Fe_2O_3 (5–45 wt%) and S (0.2–22 wt%). The Verninsky deposit rocks are more calcic (CaO ~ 4.9%) and potassic ($K_2O/Na_2O > 13.5$) compared to the Golets Vysochaishy (CaO ~ 1.5%, $K_2O/Na_2O \sim 4$) and Ikan (CaO ~ 0.6%, $K_2O/Na_2O \sim 2.6$) deposits. Barren and ore-bearing rocks of the Golets Vysochaishy deposit are similar in the Na_2O, MgO, K_2O, CaO, and Al_2O_3 contents, with slightly higher SiO_2 and extremely variable Fe_2O_3 and S abundances in the latter.

Trace element (Co, Ni, Cu, Zn, As, Cr, Zr, and Y) contents were determined for a suite of 25 whole-rock samples of ore-bearing and barren metasedimentary rocks from the Verninsky and Golets Vysochaishy deposits (Appendix A1). All the studied trace elements have highly variable contents. However, the most significant variations are detected only for those trace elements which are present in the major ore minerals (arsenopyrite, pyrite, and pyrrhotite) and are considered as mobile in the ore-forming process.

There is a significant difference in As content between ore-bearing sedimentary rocks of the Aunakit and Khomolkho Formations. Siltstones and sandstones of the Aunakit Formation from within the ore body are strongly enriched in As from 100 to 32,000 ppm (mean = 1432 ppm), whereas in the Khomolkho Formation ore-bearing rocks As varies from 1.8 to 35 ppm (mean = 18 ppm). Another feature of the host sedimentary rocks of the Verninsky deposit is that they are depleted in Co, Ni, Cu, and Zn compared to the ore-bearing Khomolkho rocks. In the Khomolkho host rocks, contents of the trace elements are on average from 2.5 (for Zn) to 8.5 (for Cu) times higher. The observed geochemical features for the ore-bearing host rocks from the Verninsky and Golets Vysochaishy deposits are largely explained by the differences in the mineral composition of the ores.

The sedimentary rocks within the Golets Vysochaishy deposit ore bodies clearly differ from the barren rocks of the Khomolkho Formation hanging wall zone by their relatively high Co, Ni, Cu, Zn, and As contents, ranging from 29 to 249 ppm (mean = 93 ppm), 54 to 390 ppm (mean = 186 ppm), 41 to 479 ppm (mean = 182 ppm), 51 to 248 ppm (mean = 136 ppm), and 1.8 to 35 ppm (mean = 18 ppm) respectively. In the barren rocks, the average values are lower: Co – 16 ppm, Ni – 42 ppm, Cu – 30 ppm, Zn – 86 ppm, and As – 4 ppm. Finally, the studied suites of ore-bearing and barren sedimentary host rocks have similar abundances of Cr, Zr, and Y.

5.3. ^{40}Ar-^{39}Ar data

The ^{40}Ar-^{39}Ar method was used to analyze three muscovite samples, two of which were separated from the late gold-bearing quartz veins of

Table 3
^{40}Ar-^{39}Ar dating results of muscovite from late quartz veins of the Golets Vysochaishy (sample Vys-2/19) and Ozherelie (sample OZh-1/10) gold deposits and granite of the Mama complex (sample Granma-1/18).

T°C	^{40}Ar(STP)	$^{40}Ar/^{39}Ar$	±1σ	$^{38}Ar/^{39}Ar$	±1σ	$^{37}Ar/^{39}Ar$	±1σ	$^{36}Ar/^{39}Ar$	±1σ	Ca/K	$\sum^{39}Ar$ (%)	Age (Ma) ±1σ	±1σ
Sample Vys −2/19, weight 12.1 mg, J = 0.004528 ± 0.000054, plateau-like age (920–1220 °C) = 331 ± 9 Ma (2σ), MSWD = 0.97													
550	4.8×10^{-9}	34.6	0.343	0.01261	0.00783	1.44	1.20	0.0435	0.0098	5.200	0.7	169.6	21.7
700	13.3×10^{-9}	47.0	0.303	0.01283	0.01219	0.47	0.42	0.0357	0.0064	1.687	2.2	275.5	13.7
810	63.5×10^{-9}	45.6	0.102	0.01565	0.00109	0.36	0.25	0.0145	0.0020	1.284	9.6	309.2	5.3
920	313.5×10^{-9}	45.94	0.043	0.01347	0.00016	0.05	0.03	0.0026	0.0008	0.179	45.6	335.7	4.0
1020	257.3×10^{-9}	46.23	0.025	0.01499	0.00097	0.001	0.07	0.0056	0.0004	0.003	75.0	331.8	3.7
1120	42.1×10^{-9}	46.77	0.055	0.01666	0.0021	0.07	0.03	0.0137	0.0011	0.239	79.8	319.0	8.2
1220	205.6×10^{-9}	54.48	0.074	0.01917	0.00078	0.01	0.09	0.0350	0.0013	0.010	99.7	328.8	4.5
1280	10.2×10^{-9}	210	1.792	0.07280	0.02184	0.30	1.88	0.6260	0.0098	1.088	100.0	196.4	18.1
Sample OZh-1/10, weight 20.1 mg, J = 0.004193 ± 0.000049, plateau-like age (700–950 °C) = 323 ± 10 Ma (2σ), MSWD = 1.7													
600	1.81×10^{-9}	370.5	10.9	0.235	0.022	0.0289	0.02	1.235	0.071	0.1	0.04	43	127
700	1.42×10^{-9}	238.6	0.29	0.096	0.002	0.0237	0.02	0.655	0.005	0.09	0.09	312	88
800	6.36×10^{-9}	66.66	0.04	0.028	0.00002	0.002	0.02	0.075	0.00008	0.01	0.89	309	8.4
850	224.5×10^{-9}	49.46	0.03	0.017	0.0001	1.19	0.3	0.008	0.00001	4.3	38.8	325	2.0
900	141.0×10^{-9}	46.74	0.06	0.015	0.0002	0.0005	0.0003	0.002	0.00003	<0.01	63.9	320	1.5
950	47.1×10^{-9}	46.76	0.06	0.016	0.0003	0.0002	0.0002	0.002	0.00004	<0.01	72.3	319	2.4
1000	34.6×10^{-9}	46.94	0.05	0.016	0.0003	0.0002	0.0002	0.003	0.00004	<0.01	78.5	319	2.9
1100	40.5×10^{-9}	46.23	0.05	0.015	0.0002	0.0002	0.0002	0.002	0.00002	<0.01	85.8	316	2.2
1200	54.5×10^{-9}	46.21	0.06	0.015	0.0005	0.0002	0.0002	0.002	0.00009	<0.01	95.6	316	2.2
1300	22.4×10^{-9}	50.97	0.30	0.018	0.0025	0.0003	0.0002	0.017	0.00083	<0.01	99.3	318	2.5
1400	3.8×10^{-9}	53.54	2.66	0.019	0.22	0.002	0.002	0.028	0.0489	0.09	99.9	313	11
1500	1.02×10^{-9}	97.43	84.5	0.045	1.34	0.13	0.1	0.26	0.49	0.5	100.0	150	55
Sample Granma-1/18, weight 19.09 mg, J = 0.005992 ± 0.000094, plateau age (800–1050 °C) = 308 ± 11 Ma (2σ), MSWD = 0.64													
550	1.4×10^{-9}	17.10	0.52	0.0408	0.0287	8.67	6.29	0.0563	0.0297	31.2	0.3	4.9	94.4
700	9.8×10^{-9}	36.46	0.46	0.0217	0.0088	2.26	1.82	0.0622	0.0124	8.1	1.1	185.6	35.8
800	27.2×10^{-9}	40.51	0.12	0.0140	0.0028	0.83	0.31	0.0358	0.0030	3.0	3.2	297.6	9.2
900	112.4×10^{-9}	34.74	0.06	0.0119	0.0016	0.04	0.39	0.0134	0.0018	0.2	13.4	305.2	6.5
990	561.7×10^{-9}	32.39	0.02	0.0112	0.0004	0.08	0.06	0.0036	0.0006	0.3	67.9	310.2	4.8
1050	191.1×10^{-9}	32.26	0.03	0.0113	0.0006	0.28	0.13	0.0031	0.0008	1.0	86.6	310.5	5.0
1120	42.8×10^{-9}	32.46	0.08	0.0117	0.0008	0.47	0.22	0.0121	0.0023	1.7	90.7	287.9	7.6
1250	96.9×10^{-9}	32.81	0.09	0.0130	0.0010	0.03	0.23	0.0100	0.0028	0.1	100.0	296.9	8.7

J – characteristic of the neutron flux during irradiation of samples.

the Golets Vysochaishy (Vys-2/19) and Ozherelie (Ozh-1/10) deposits, and one sample (Granma-1/18) - from a garnet - muscovite granite of the Mama complex. The results are given in Table 3 and plotted in the age spectra and $^{36}Ar/^{40}Ar$ vs. $^{39}Ar/^{40}Ar$ (inverse isochron) diagrams in Fig. 6.

The Vys-2/19 muscovite sample (Fig. 6a) is characterized by a continuous increase in apparent ages at the initial part of the $^{40}Ar/^{39}Ar$ spectrum. At the low-temperature (550 – 810° C) steps (ca. 10% of the ^{39}Ar released), the apparent $^{40}Ar/^{39}Ar$ ages range from 170 to 310 Ma. For these steps, an inverse correlation is observed between T and the Ca/K ratio, which decreases from 5.2 to 1.3 as the temperature increases. The spectrum also has a sub-horizontal segment, which is identified for the middle and high-temperature (920–1220 °C) steps. It includes 4 successive steps, with 90.1% of the ^{39}Ar released and yields a plateau-like age of 331 ± 9 Ma (2σ, MSWD = 0.97) (Fig. 6a). These steps also show low Ca/K values (<0.24). In the $^{39}Ar/^{40}Ar$ vs $^{36}Ar/^{40}Ar$ diagram, the data points corresponding to these steps yield an isochron with an age of 332 ± 14 Ma (2σ, MSWD = 4.5) and a $(^{40}Ar/^{36}Ar)_i$ value of 265 ± 24, which is close to that for atmospheric argon (Fig. 6b).

Step-heating analysis of the Ozh-1/10 sample yields a relatively wide range of apparent ages from 100 to 326 Ma. There is a continuous decrease in the apparent ages for most of the spectrum (c. 99% of the ^{39}Ar released). The Ca/K ratio in almost all temperature fractions does not exceed 0.5. An exception is the argon fraction obtained at 800 °C heating step, for which Ca/K = 4.3. This step yields the highest $^{40}Ar/^{39}Ar$ age of 326 Ma, which may indicate the presence of excess ^{40}Ar. In the temperature range of 800–950 °C, the Ozh-1/10 sample spectrum demonstrates sub-horizontal segment with a plateau-like age of 323 ± 10 Ma (2σ, MSWD = 1.7). It includes 5 sequential steps with 63.9% of the ^{39}Ar released. In the inverse isochron diagram, the regression line through all five data points corresponds to an age of 322 ± 9 Ma (2σ, MSWD = 9) and the $(^{40}Ar/^{36}Ar)_i$ value of 272 ± 37, identical, within uncertainty, to the atmospheric ratio (Fig. 6c).

Muscovite from the Mama complex granite exhibits a complex age spectrum. The apparent age rises to a maximum value at the initial heating steps (550–800 °C, ~3% of the ^{39}Ar released) and then forms an extended plateau in the middle segment of the spectrum. The higher temperature steps (1120 and 1250 °C, ~ 10% of ^{39}Ar released) produce younger apparent age. The plateau includes 4 sequential steps ranging from 800 to 1050 °C and combines 85.5% of the ^{39}Ar released (Fig. 6e). The $^{40}Ar/^{39}Ar$ age, calculated from these steps, is 308 ± 11 Ma (2σ, MSWD = 0.64). Thus, it satisfies most criteria for a plateau age (Fleck et al., 1977; Baksi 1999; 2006). The inverse isochron method yields a similar age of 312 ± 9 Ma (2σ, MSWD = 0.3) and a $(^{40}Ar/^{36}Ar)_i$ value of 250 ± 45 (Fig. 6f).

5.4. *Summary of the ^{40}Ar-^{39}Ar ages for the muscovite from late quartz veins*

As was shown above, the muscovite samples from the late quartz veins of the Golets Vysochaishy and Ozherelie deposits have discordant (staircase-shaped) age spectra, which are difficult to interpret. For

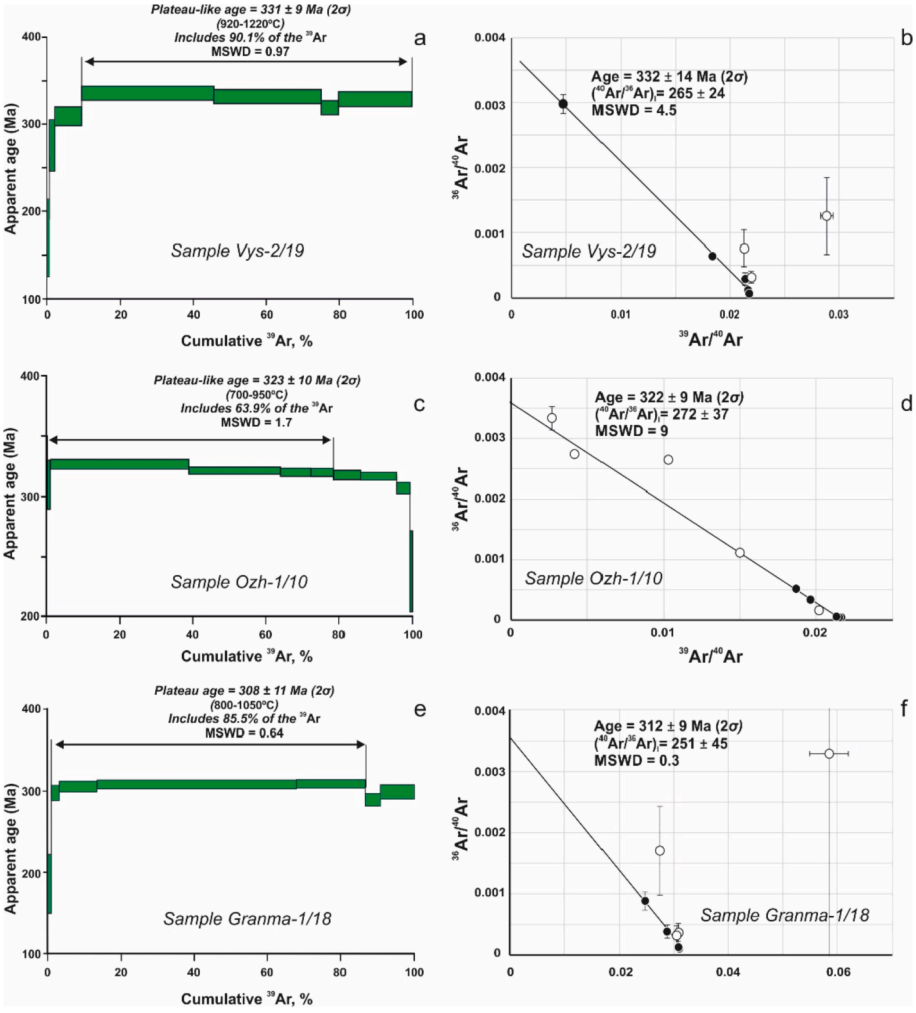

Fig 6. $^{40}Ar/^{39}Ar$ age spectra and $^{36}Ar/^{40}Ar$ vs. $^{39}Ar/^{40}Ar$ correlation (inverse isochron plots) diagrams for muscovite from gold-bearing quartz veins of the (a,b) Golets Vysochaishy (Vys-2/19) and (c, d) Ozherelie (Ozh-1/10) deposits, and (e, f) muscovite (Granma-1/18) from a garnet - muscovite granite of the Mama complex.

micas, the staircase shape of a spectrum reflects the formation of secondary reaction products (Hess et al., 1987; Villa, 2021, and references therein).

All ^{40}Ar-^{39}Ar spectra obtained have extended age plateaus. The defined plateaus satisfy some criteria of Fleck et al. (1977) and Baksi (1999, 2006) to be considered as such, including: 1) the plateaus comprise >3 sequential temperature steps, combining >60% of ^{39}Ar gas released; 2) the $^{40}Ar/^{39}Ar$ plateau data yield p values of >0.05 (95% confidence level); and 3) the plateau ages are consistent with the inverse isochron ages. At the same time, the samples Vys-2/19 and OZh-1/10 have relatively scattered steps included in calculation of the plateau and inverse isochron ages. The scatter leads to up to 4% errors on the plateau and inverse isochron ages, and high MSWD of up to 9. In this instance, calculated plateau ages should be considered plateau-like (or pseudo-plateau) ages. However, the plateau-like ages obtained agree with the Rb-Sr isochron ages and, thus, can be considered to be reliable.

The Vys-2/19 muscovite $^{40}Ar/^{39}Ar$ age spectrum has an ascending staircase shape; the sample has Ca/K ratios that inversely correlate with the apparent ages in the low temperature steps. These features are generally explained by the presence of poorly crystallized alteration phases with younger ages (Wijbrans and McDougall, 1986; Ruffet et al., 1996; Iwata & Kaneoka, 2000 and references cited therein). Optical microscopy did not reveal any distinct signs of alteration of the sample. However, the presence of micro-sized mineral phase inclusions of secondary minerals in white micas (Villa et al., 1996; Villa, 2021), cannot be entirely excluded. Another cause for the scatter of the data may be partial disturbance of the K-Ar isotope system in the muscovite, although this possibility does not explain all of its age spectrum features.

The OZh-1/10 age spectrum is characterized by a continuous decrease in apparent ages from the middle to high temperature steps. The descending staircase age spectrum may indicate the presence of excess ^{40}Ar (Lanphere & Dalrymple, 1976; Kelley, 2002). In some cases, the loss of ^{39}Ar by recoil has been shown to be responsible for higher apparent ages. Onstott et al. (1995) and Villa (1997) pointed out that this mechanism is most effective in fine-grained mineral phases such as those present in clays. It this study we analyzed coarse-grained aggregates of the muscovite (Fig. 5f), and, thus, conclude that the recoil loss is the least probable explanation. The excess ^{40}Ar can be present in minerals formed in closed, fluid-poor systems (Kelly, 2002). However, according to the petrographic observations, the OZh-1/10 muscovite sample most likely crystallised in a fluid-rich, open hydrothermal system. Thus, the slightly overestimated apparent step ages of the middle temperature segment may be explained by a minor K loss from muscovite during a superimposed hydrothermal event, as has been also reported by Villa (2021). This assumption is consistent with the high Ca/K = 4.3 at the 800 °C step that has a maximum apparent age. The sample shows evidence of a superimposed low-temperature processes such as replacement of carbonates by iron hydroxides.

5.5. The Rb-Sr data

The Rb-Sr isotopic data are presented in Table 4 and plotted in Fig. 7. Whole-rock samples of the veinlet-disseminated ores from the Verninsky, Golets Vysochaishy, and Ikan deposits show significant variations of the Rb and Sr concentrations from 19 to 455 ppm and 32 to 680 ppm, respectively. As a results, the $^{87}Rb/^{86}Sr$ and $^{87}Sr/^{86}Sr$ ratios in these samples also vary in a wide range: from 0.087 to 5.22 and from 0.7122 to 0.7701, respectively. Notably, the low $^{87}Rb/^{86}Sr$ ratios are more typical of the whole-rock samples from the Verninsky deposit, while those from the Golets Vysochaishy and Ikan deposits demonstrate systematically higher values. These differences are caused by the presence of different amounts of carbonate minerals in the ore-bearing host rocks of these deposits. The proportions of carbonate in the sandstones and carbonaceous siltstones of the Aunakit Formation hosting Verninsky deposit are (up to vol. 20%) higher, compared to rocks from the other two deposits, where the amounts of carbonate minerals do not exceed

Table 4
Rb-Sr isotope data for whole-rock samples and mineral separates from gold-bearing ores of the Shukhoi Log-style deposits (Bodaibo District, Northern Transbaikalia).

№	Sample	Sample description	Rb, ppm	Sr, ppm	$^{87}Rb/^{86}Sr$	$^{87}Sr/^{86}Sr$ (2SE)
Verninsky deposit						
early veinlet-disseminated sulfide mineralization						
1	V-2/10	whole-rock	106	306	1.00	0.718017 ± 22
2		F-fraction	184	259	2.05	0.724585 ± 10
3		H-fraction	102	345	0.857	0.717167 ± 11
4	V-3/10	whole-rock	132	102	3.75	0.734719 ± 22
5		F-fraction	125	93	3.89	0.735615 ± 17
6		H-fraction	100	115	2.52	0.727162 ± 11
7	V-5/10	Same	20	680	0.087	0.712160 ± 21
8	V-7/10	Same	51	233	0.630	0.715603 ± 21
9	V-7/10a	Same	51	238	0.619	0.715524 ± 21
10	V-14/10	Same	90	361	0.723	0.715850 ± 21
Golets Vysochaishy deposit						
early veinlet-disseminated sulfide mineralization						
11	Vch-1/10	whole-rock	155	125	3.60	0.735067 ± 11
12	Vch-9/10	Same	111	80	3.99	0.739326 ± 12
13	Vch-13/10	Same	169	136	3.61	0.734237 ± 11
14	Vch-15/10	Same	148	159	2.69	0.729846 ± 10
15	Vch-17/10	Same	80	163	1.42	0.722329 ± 13
16	Vch-19/10	Same	46	154	0.856	0.718613 ± 10
17	Vch-22/10	Same	455	298	4.42	0.739969 ± 13
18	V-03-14	Same	58	219	0.764	0.716916 ± 18
19	V-03-22	Same	85	190	1.28	0.721455 ± 14
20	V-03-23	Same	72	76	2.74	0.730497 ± 15
21	V-03-24	Same	101	74	3.94	0.737149 ± 15
22	V-03-25	Same	19	31.7	1.71	0.723607 ± 15
23	V-03-26	Same	103	147	2.03	0.726577 ± 14
late gold-bearing quartz vein						
24	Vys-2-19	muscovite	407	225	5.23	0.743993 ± 12
25		whole-rock	250	480	1.51	0.726161 ± 13
26		F-fraction	271	444	1.77	0.727545 ± 10
27		H-fraction	219	531	1.19	0.724755 ± 11
28	Vys-3/19	muscovite	422	248	4.93	0.742818 ± 12
29		F-fraction	267	462	1.68	0.727122 ± 12
30		H-fraction	175	633	0.799	0.722696 ± 10
31	Vys-4/19	muscovite	315	172	5.30	0.744665 ± 10
32		Same	373	181	5.95	

(*continued on next page*)

Table 4 (*continued*)

N°	Sample	Sample description	Rb, ppm	Sr, ppm	$^{87}Rb/^{86}Sr$	$^{87}Sr/^{86}Sr$ (2SE)
	GV-3/18					0.747133 ± 11
33	GV-5/18	Same	370	215	4.98	0.743040 ± 10
Ozherelie deposit						
late gold-bearing quartz vein						
34	Ozh-1/18	carbonate and minor muscovite	101	764	0.384	0.711953 ± 10
35		Same	444	396	3.25	0.725563 ± 10
36	Ozh-2/18	carbonate and minor muscovite	132	501	0.758	0.713608 ± 10
37	Ozh-3/18	muscovite	494	502	2.85	0.723710 ± 10
38	Ozh-4/18	Same	317	373	2.45	0.722100 ± 10
Ikan deposit						
early veinlet-disseminated sulfide mineralization						
39	IK-70	whole-rock	125	69.2	5.22	0.770064 ± 11
40		muscovite + chlorite	214	82.4	7.50	0.781964 ± 10
41	IK-72	whole-rock	89	79.6	3.24	0.761114 ± 11
42		muscovite + chlorite	164	71.7	6.64	0.777081 ± 11
late gold-bearing quartz vein						
43	Ikan-3/18	chlorite	0.644	0.441	4.23	0.765637 ± 33
44	Ikan-7/18	chlorite and minor muscovite	4.96	1.33	10.81	0.796804 ± 10
45	Ikan-7/18	chlorite and minor muscovite	8.08	1.65	14.18	0.813798 ± 13

2–3 vol%.

In addition to the whole-rock samples, eight mineral concentrates were studied for the Rb-Sr isotope systematics. These concentrates were obtained for two samples of the veinlet-disseminated sulfide ores from the Verninsky and for two samples of quartz-sericite metasomatites located at the contact of quartz veins at the Golets Vysochaishy deposit. Concentrates of the F-fraction generally have a higher content of Rb and a lower content of Sr than those of the H-fraction and the whole-rock samples (Table 4). As a result, the $^{87}Rb/^{86}Sr$ ratio in the F-fractions is systematically higher (by factor of 1.5–2.4) than in the heavy fraction. These differences are caused by the enrichment of the float fraction in sericite, while other rock-forming minerals, including carbonate, are dominantly concentrated in the heavy fraction. The $^{87}Rb/^{86}Sr$ and $^{87}Sr/^{86}Sr$ ratios for the float and heavy fractions vary from 0.8 to 3.9 and 0.7172 to 0.7356, respectively. These ratios are within the range determined for the whole-rock samples.

Compared to the whole-rock samples and mineral fractions, mineral separates and their mixtures show significantly wider ranges of $^{87}Rb/^{86}Sr$ (0.4–14.2) and $^{87}Sr/^{86}Sr$ (0.7119–0.8138) (Table 4). Muscovite separates obtained from the late quartz veins of the Golets Vysochaishy and Ozherelie deposits show a narrow range of Rb contents (315–494 ppm) and a a wide range of Sr concentrations (172–502 ppm). Such high and heterogeneous Sr contents in muscovite separates are explained by the presence of small amounts (<5%) carbonate minerals in the separates. The lowest contents of Rb (0.6 ppm) and Sr (0.4 ppm) were found in the chlorite separates from the late quartz veins of the Ikan deposit. In mineral separate mixtures (carbonate + muscovite and chlorite + muscovite), the Rb and Sr contents vary from 5 to 214 and 1.3 to 769 ppm, respectively.

5.5.1. The Verninsky deposit

In the Rb-Sr isochron diagram (Fig. 7a), the data points for 6 whole-rock samples and 4 mineral separates from veinlet-disseminated sulfide ores of the Verninsky deposit define a regression line with an apparent age of 440 ± 8 Ma (2σ) and initial $^{87}Sr/^{86}Sr$ of 0.7117 ± 0.0002 (n = 10, MSWD = 23). The data for the whole-rocks and mineral separates of samples V-2/10 and V-3/10 only define a better constrained isochron with a similar age of 434 ± 4 Ma ($^{87}Sr/^{86}Sr_i$ = 0.71195 ± 0.00008, n = 6, MSWD = 2.2).

5.5.2. The Golets Vysochaishy deposit

For the Golets Vysochaishy deposit, the Rb-Sr data obtained can be subdivided into two groups (Fig. 7b,c). The first group is represented by whole–rock samples of the veinlet-disseminated sulfide mineralization. The data for the first group plot with a significant scatter (MSWD = 136) and in the Rb-Sr isochron diagram define a regression line with slope corresponds to an age of 439 ± 27 Ma (2σ) and $(^{87}Sr/^{86}Sr)_i$ = 0.7133 ± 0.0011 (Fig. 7b). The data for the second group represented by whole-rock samples and mineral separates from quartz-sericite metasomatites of the late quartz veins yield a better constrained (MSWD = 5) isochron with a significantly younger age of 342 ± 5 Ma (2σ) and a higher $(^{87}Sr/^{86}Sr)_i$ = 0.7190 ± 0.0002 (Fig. 7c).

5.5.3. The Ozherelie deposit

For the Ozherelie deposits, five muscovite separates from the late gold-bearing quartz vein were analyzed for the Rb-Sr isotope systematics. The data for the separates define a regression line with a slope corresponding to an age of 344 ± 15 Ma (2σ), $(^{87}Sr/^{86}Sr)_i$ = 0.7101 ± 5, and MSWD = 13 (Fig. 7d).

5.5.4. The Ikan deposit

For the Ikan deposit, Rb-Sr data were obtained for whole-rock samples of the veinlet-disseminated sulfide ores and for the late quartz veins. In the Rb-Sr isochron diagram, these data plot with a moderate scatter (MSWD = 5.8) and define a regression line with a slope corresponding to an age of 344 ± 8 Ma (2σ) and an initial $^{87}Sr/^{86}Sr$ = 0.7453 ± 9.

5.6. Summary of the Rb-Sr data the heterogeneity of the initial Sr isotopic composition

The Rb-Sr isotopic results obtained in this study demonstrate a common feature, namely a substantial scatter (MSWD of up to 136) of the data points in the Rb-Sr isochron diagrams. The highest values of the MSWD were obtained for the whole-rocks samples of the early veinlet-disseminated sulfide ores of the Verninsky (MSWD = 23) and Golets Vysochaishy (MSWD = 136) deposits. For the other deposits, the MSWD values are significantly smaller and do not exceeding 13. In this study, the parameters of the isochrons were calculated using the method of York (1966). It allows obtaining the correct ages even for the increased data characterized by large dispersion. Data scatter mainly affects an error on the calculated Rb-Sr age and the initial $^{87}Sr/^{86}Sr$ (York, 1966; Kostitsyn, 1989).

The generally large scatter of the Rb-Sr data in the isochron diagrams beyond the analytical uncertainties can be due to several reasons. One of the reasons could be the heterogeneity of the initial Sr isotopic composition in the ore-forming fluid and/or an incomplete homogenization of the Rb-Sr isotope system between the metasomatic minerals of the altered ore-bearing rocks. The $\delta^{18}O$ data for quartz and altered metasedimentary rocks at the Sukhoi Log deposit (Dubinina et al., 2014) indicate that the ore-forming system had a low fluid/rock ratio (W/R ≤ 0.2). This suggests the fluid migration in micropores and micro-dislocation space (cleavage, micro-fractures), which is also confirmed

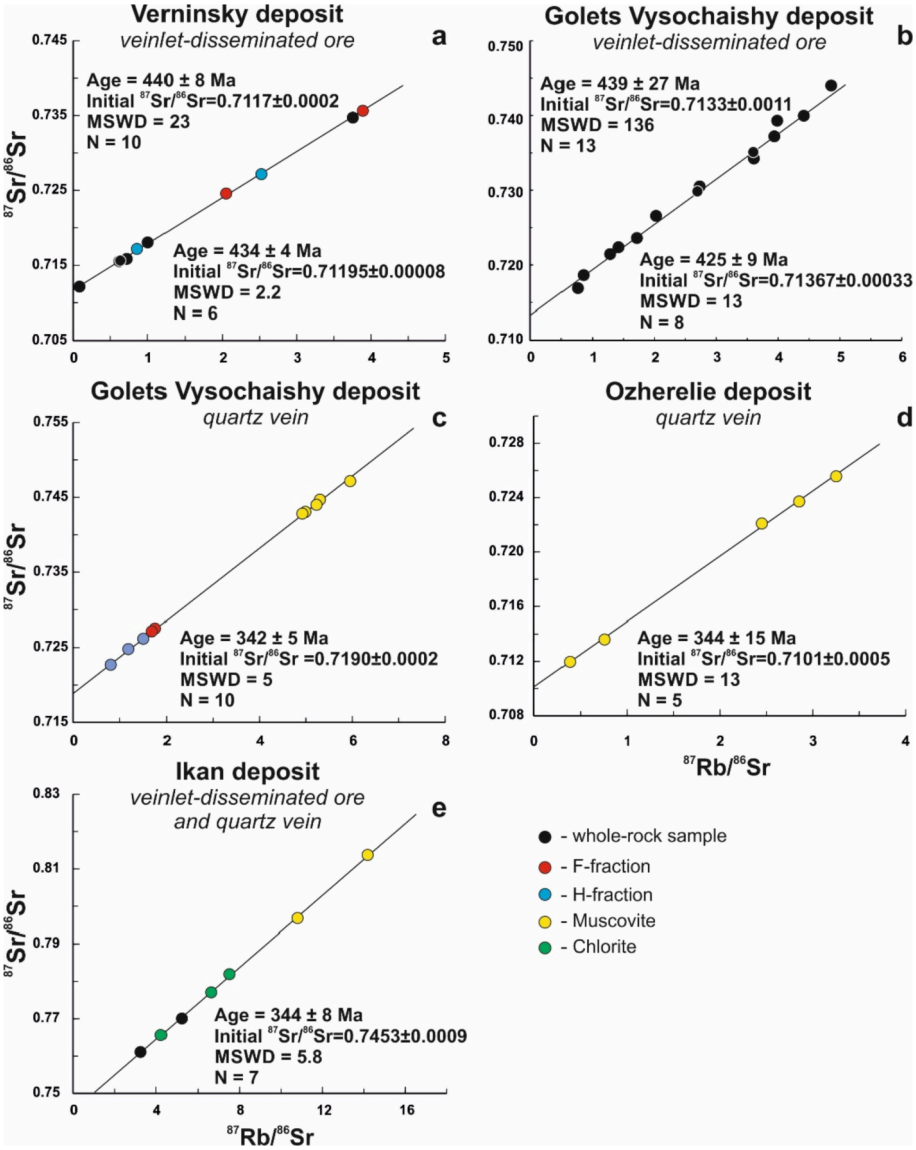

Fig. 7. Rb–Sr isochron diagrams for veinlet-disseminated sulfide ores and quartz veins from the Sukhoi Log-style deposits.

by microscopic observations both at the Sukhoi Log and at other deposits of the Sukhoi Log-type (Large et al., 2007; Rusinov et al., 2008; Tarasova et al., 2020; Tarasova et al., 2021, etc.). Such ore-forming systems may have some variations of the P-T conditions under which they formed and, possibly, also isotopic parameters (Rusinov et al., 2008; Chugaev et al., 2014; Dubinina et al., 2010; 2014; Prokof'ev et al., 2019).

The heterogeneity of the initial Sr isotopic composition as the main reason for larger scatter of the data is indicated by the data on the veinlet-disseminated sulfide ores from the Verninsky deposit. The regression of the combined data for all ten samples analysed yields the maximum amount of scatter as evidenced by MSWD = 23. However, when regressing the data for samples V-2/10 and V-3/10 only (both the whole-rock and mineral separates), the scatter of the data is reduced significantly (MSWD = 2.2). Notably, samples V-2/10 and V-3/10 were collected within the same ore body, <1 m apart from each other. A significant decrease in the MSWD value shows that the isotopic equilibrium, caused by hydrothermal alteration of the host rocks, was reached locally within the ore body, but was not attained within the entire volume of the ore body. Additionally, the similarity, within the uncertainties of the ages (440 ± 8 and 434 ± 4 Ma), derived from both isochrons, suggests that the "residual" heterogeneity of the Rb-Sr system components of the ore-bearing rocks does not significantly affect the reliability of the dating results. In terms of the parameters of the isochrons (T = 434 ± 4 Ma (2σ), $(^{87}Sr/^{86}Sr)_i$ = 0.71195 ± 0.00008), the regression line obtained for samples V-2/10 and V-3/10 is more reliable and is further considered as the age of the veinlet-disseminated sulfide mineralization of the Verninsky deposit.

Interpretation of the Rb-Sr data for the veinlet-disseminated sulfide ores of the Golets Vysochaishy deposit is more complicated. In general, the data for the whole-rock samples of the ore-bearing rocks plot with a large scatter in the isochron diagram (MSWD = 136). The studied samples were collected within the same ore body, but at different locations. These samples have different sulfide abundances, possibly as a result of variable degrees of hydrothermal alteration. For example, in samples V-03-14 and V-03-19, the sulfide mineralization is represented by isolated small lenticular grains of pyrrhotite, while in sample V-03-24, there is a sulfide veinlet containing coarse-grained euhedral pyrite in association with pyrrhotite grains (Fig. 5c, d). However, it is difficult to assess the degree of alteration for the metasediments caused by ore-forming processes from macro- and microscopic observations only. The problem can be approached via using the degree of variability of trace elements in the ore-bearing rocks (Appendix A1). Using this approach, we compared the studied samples from the ore zone with the barren host rocks of the Khomolkho Formation. The parameters used

were the concentration ratios of the traditionally mobile (Ni, Cu, As) and immobile (Y, Zr) elements in ore-forming processes. These elements were selected because Co, Ni, and As are concentrated mainly in pyrite and pyrrhotite, the main ore minerals of the veinlet-disseminated sulfide ores of the deposit, while Cu is mainly present in chalcopyrite (Large et al., 2007; Tarasova et al., 2021).

The barren metasedimentary rocks of the Khomolkho Formation sampled at a significant (>10 km) distance from the Golets Vysochaishy deposit demonstrate low and moderately variable Ni/Y (0.5–2.0) and Cu/Zr (0.14–0.32) ratios (Chugaev et al., 2018) (Fig. 8a, b). The mildly altered barren host rocks sampled at the deposit from the hanging wall zone have similar Ni/Y and Cu/Zr ratios that vary in somewhat wider ranges from 0.7 to 8.4 and 0.1 to 0.5, respectively.

In the Ni/Y vs. Cu/Zr diagram (Fig. 8a), the Khomolko Formation samples collected far away from the mineralization form a compact field at the low end of the ratios. In contrast, samples from the ore zone show wide ranges in both Ni/Y (2–34) and Cu/Zr (0.15–2.2), as well as in As/Y (0.14–5.4, Fig. 8b) and plot along a trend, with the field for the barren sedimentary rocks of the Khomolkho Formation plotting near the lower end of the trend. At the same time, some of the studied samples are close in Ni/Y and Cu/Zr ratios to the mildly altered barren rocks of the Khomolkho Formation, while the other samples differ and show systematically higher values of Ni/Y (≥10) and Cu/Zr (≥0.5). The chemical

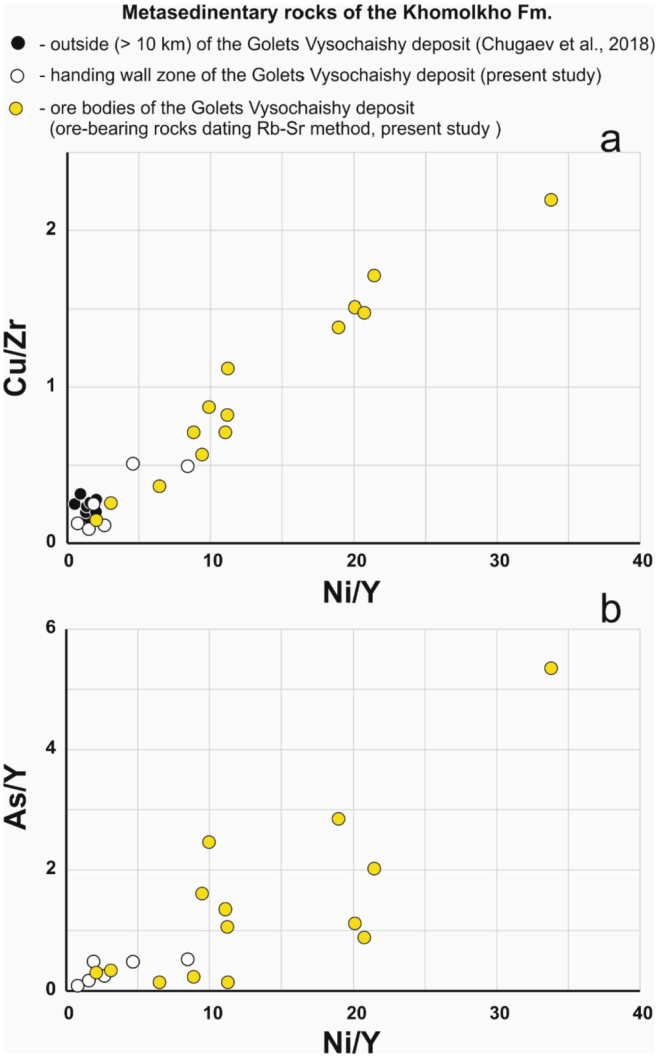

Fig. 8. Ni/Y vs. Cu/Zr (a) and Ni/Y vs. As/Y diagrams for barren and ore-bearing metasedimentary rocks of the Khomolkho Formation from the Golets Vysochaishy deposit.

heterogeneity of the samples selected for the Rb-Sr analysis is also evident in the Ni/Y vs. As/Y diagram (Fig. 8b). The samples include rocks with a low As/Y (0.14–0.33) ratio. In this diagram, their data points plot either in the field of the mildly altered barren rocks of the Khomolkho Formation (As/Y = 0.06–0.53) or close to it.

Thus, the studied samples of the veinlet-disseminated sulfide ores from the Golets Vysochaishy deposit show a different degree of alteration by the ore-forming fluid. Based on the above parameters (e.g., Ni/Y > 10, Cu/Zr > 0.5, As/Y > 1), a group of 8 samples characterized by the maximum degree of hydrothermal-metasomatic alteration was identified. In the Rb-Sr diagram, the data for this group of samples plot with a moderate scatter (MSWD = 13) and define a regression line with a slope corresponding to an age of 425 ± 9 Ma (2σ) and $(^{87}Sr/^{86}Sr)_i$ = 0.71367 ± 0.00033. We consider these data as the most accurate estimate of the age of the early veinlet-disseminated sulside mineralization in the Golets Vysochaishy deposit. Likewise, for the Verninsky deposit, the whole-rock samples of the veinlet-disseminated sulfide ores from the Golets Vysochaishy deposit demonstrate a good agreement between the Rb-Sr age obtained for the entire dataset and the one calculated for the selected group of the 8 samples.

6. Discussion

6.1. Age of the gold mineralization in the Sukhoi Log-type deposits

The results of the age determinations for the gold mineralization of the Sukhoi Log-type ore deposits are compiled in Table 5. The analysis of the ^{40}Ar-^{39}Ar and Rb-Sr geochronological dataset obtained for the four deposits studied allowed us to distinguish two separate groups of ages.

The first group of the older, Silurian ages, is obtained for the veinlet-disseminated sulfide mineralization of the Verninsky (434 ± 4 Ma) and Golets Vysochaishy (425 ± 9 Ma) deposits. The ages are similar to, although somewhat younger than, the ages of the veinlet-disseminated sulfide ores of the Sukhoi Log deposit obtained earlier by the Rb-Sr (454 ± 6 Ma) and U-Th-Pb SHRIMP (439 ± 17 Ma) methods (Laverov et al., 2007; Yudovskaya et al., 2011). These deposits are located at a significant distance from each other, occurring in different tectonic blocks and stratigraphic units of the Precambrian metasediments of the BPB (Figs. 2 and 3). The similarity of the ages for the same ore type allows us to propose the presence of a Silurian (450–430 Ma) ore-forming event in the region.

The second group of significantly younger, Carboniferous ages, have been obtained for the late quartz veins of the Golets Vysochaishy and

Table 5
Comparison of the ages for gold-bearing mineralization of the Sukhoi Log-style deposits.

Deposit	Gold mineralization	Method	Age ± 2SD, Ma
Verninsky	veinlet-disseminated sulfide ore	Rb-Sr (mineral + whole-rock isochron, 6 pts.)	434 ± 4
Golets Vysochaishy	veinlet-disseminated sulfide ore	Rb-Sr (mineral + whole-rock isochron, 8 pts.)	425 ± 9
	quartz vein	$^{40}Ar/^{39}Ar$ (muscovite)	331 ± 9
		Rb-Sr (mineral + whole-rock isochron, 10 pts.)	342 ± 5
Ozherelie	quartz vein	$^{40}Ar/^{39}Ar$ (muscovite)	323 ± 10
		Rb-Sr (mineral isochron, 5 pts.)	344 ± 15
Ikan	veinlet-disseminated sulfide ore + quartz vein	Rb-Sr (mineral + whole-rock isochron, 7 pts.)	344 ± 8

Ozherelie deposits, as well as for the Ikan deposit mineralization. The Rb-Sr and ^{40}Ar-^{39}Ar ages obtained for this group generally coincide within their respective uncertainties. However, we consider the Rb-Sr results as more reliable estimation of age of the gold-bearing vein mineralization. This is due to the fact that the Rb-Sr isochrons were obtained for the more representative set of whole-rock samples and mineral separates compared to the ^{40}Ar-^{39}Ar results obtained on single minerals. Additionally, the ^{40}Ar-^{39}Ar age spectra were shown to be likely disturbed and, therefore, the plateau-like ages may be compromised. The Rb-Sr isotope system in muscovite is generally considered to be more resistant to superimposed processes in comparison to the K-Ar system (Dodson, 1979; Cliff, 1985; Szczerba et al., 2015). Thus, we consider the Rb-Sr isochron data for the Golets Vysochaishy (342 ± 5 Ma) and Ozherelie (344 ± 15 Ma) deposits as the best estimates for of age of the late quartz veins..

Regarding the Rb-Sr data for the Ikan deposit, the veinlet-disseminated and vein mineralization samples plot on a common isochron with an age of 344 ± 8 Ma. This allows us to suggest that later processes resulted in re-equilibration of the Rb-Sr system in the minerals composing the veinlet-disseminated sulfide ores. This conclusion is confirmed by the field observations and the results of optical microscopy, indicating intensive alteration of the early vein-disseminated sulfide ores during formation of the late quartz veins. Accordingly, the Rb-Sr data for the Ikan deposit reflect the age of the Carboniferous event, which corresponds to the age of formation of the quartz veins. The age of this late event can be approximated as being within the 340–330 Ma interval, based on the Rb-Sr data for the Golets Vysochaishy (342 ± 5 Ma) and Ikan (344 ± 8 Ma) deposits. These Rb-Sr data have best age errors (1.5 and 2%, 2SD) and lower of MSWD (5.0 and 5.8) (Table 5). The presence of the Carboniferous thermal event at the Ozherelie and Ikan deposits is supported by the Rb-Sr data of Neymark et al. (1990). Pegmatite veins in the Bodaibo District are also of the Middle Carboniferous age (327 ± 5 Ma).

The ^{40}Ar-^{39}Ar age of 308 ± 11 Ma for the muscovite from the Mama complex garnet-muscovite granite of appears to be too young. Earlier, Zorin et al. (2008) dated the complex at 421 ± 15 Ma by the U-Pb SHRIMP technique on zircon. The discrepancy between the ^{40}Ar-^{39}Ar and U-Pb data may be explained by the complete "reset" of the K-Ar system in the muscovite during the Carboniferous thermal event. However, the analyzed zircon from the Mama complex granite has a high U content of ~2000 ppm. According to White and Ireland (2012), U-Pb SHRIMP dating of such zircon may yield ages too old. The observed inconsistency between the different age determinations imply that the age of the Mama complex age still needs to be confirmed, although the U-Pb data are consistent with the general geological framework. Here, we consider the most likely age of the Mama complex to be Early Paleozoic.

The geochronological data obtained indicate, therefore, that the late gold-bearing quartz veins in the Bodaibo District were formed in the Middle Carboniferous. A similar age was previously obtained for the late gold-bearing quartz veins at the Sukhoi Log (326 ± 14 Ma) and Golets Vysochaishy (331 ± 9 Ma) deposits (Laverov et al., 2007; Tarasova et al., 2021).

In summary, two ore-forming events were recognized based on the results of the present geochronological study of the gold mineralization in the four different Sukhoi Log-style gold deposits (Fig. 9a,b). In the Silurian event (450–430 Ma), the veinlet-disseminated sulfide ores, having the main economic significance, were formed. During the Middle Carboniferous (ca. 340–330 Ma) event, the rejuvenation of the ore processes led to the formation of the gold-bearing quartz veins, which have a limited economic significance in terms of the gold reserves.

6.2. *Age correlation of the ore-forming events and the Paleozoic tectonic setting of the BPB*

The main features of the Paleozoic geological evolution and tectonic settings of the Baikal-Patom fold belt and adjacent tectonic blocks were considered in detail in Zorin et al. (2008), Yarmolyuk et al. (2012), Donskaya et al.(2013), Kröner et al. (2014), and Tsygankov et al. (2017). According to the existing concepts, the Paleozoic tectonic evolution of the BPB included the collision and post-collision stages.

During the Caledonian period (prior to Devonian), the Precambrian blocks of the CAOB's continental crust, along with the Early Paleozoic island arcs and the ophiolite complexes of the Paleo-Asian Ocean, have been accreted to the Siberian Craton. These processes were accompanied by metamorphism and formation of the *syn*-metamorphic granitoid intrusions (Donskaya et al., 2013 and references cited therein). Based on the U-Pb ages of zircon from the *syn*-metamorphic granites and metamorphic monazite in the metasedimentary rocks, the BPB was affected by multiple stages of regional metamorphisme that occurred from the Cambrian to the Late Silurian (520–420 Ma, Meffre et al., 2008; Zorin et al., 2008; Donskaya et al., 2013). The Rb-Sr isochron ages obtained for the Sukhoi Log-type deposits in this study are close to the younger limit of this time interval. They coincide with the U-Pb zircon age of 421 ± 15 Ma for the S-type granites of the Mama complex exposed in the immediate vicinity of the Ozherelie and Ikan deposits. Thus, the formation of the veinlet-disseminated sulfide ores occurred at the post-peak stage of the regional metamorphism. This conclusion is consistent with the results of the mineralogical and microstructural studies of the veinlet-disseminated sulfide ores of the Sukhoi Log and Krasniy deposits. They showed that the formation of the majority of the gold-bearing sulfides in the early ores occurred during the metamorphic transformation and ductile deformation of the host sedimentary rocks (Large et al., 2007; Tarasova et al., 2020). It is possible that there was an earlier ore-formation stage (catagenesis or early episodes of metamorphism of the sedimentary sequence, Large et al., 2007) during which primary ores might also have formed. In this case, the Rb-Sr ages of the veinlet-disseminated sulfide ores correspond to the timing of late

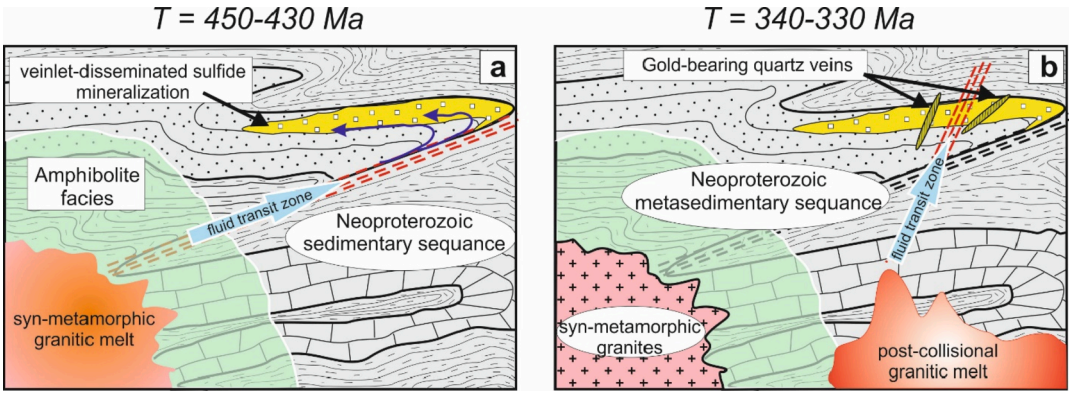

Fig. 9. (a,b). Schematic two-stage model for the formation of the Sukhoi Log-style gold deposits from the Bodaibo District (Northern Transbaikalia, Russia).

metamorphic re-mobilization and concentration of gold.

During the Hercynian period, when the gold-bearing quartz veins were formed, there was a large-scale reworking of the lithosphere of the southern margin of the Siberian continent accompanied by the supra-subduction zone granitoid magmatism. The latter produced the Middle Carboniferous - Early Permian giant (>150,000 km^2) composite Angara - Vitim batholith (Tsygankov et al., 2010; 2017; Donskaya et al., 2013). Its formation occurred over a wide time interval, from 330 to 280 Ma. At the same time, the major phases of the granitoid magmatism occurred during the period of 320–290 Ma and were associated with the formation of large-scale autochthonous and allochthonous intrusions of calc-alkaline granites. Our geochronological data on the gold-bearing quartz veins (340–330 Ma) are in good agreement with the U-Pb zircon ages of 330–325 Ma for the early phases of the Angara-Vitim granitic magmatism that took place near the Sukhoi Log, Ikan and Ozherelie deposits (Fig. 2; Tsygankov et al., 2010; 2017).

The contemporary occurence of the granitoid magmatism and the ore-forming processes may indicate a genetic relationship between the two events. However, the existing Pb, Sr, Nd, O, C, and S isotopic data for the ore and gangue minerals from the late quartz veins indicate that the sedimentary host rocks were the dominant source of the ore-forming components (Rusinov et al., 2008; Chernyshev et al., 2009; Chugaev & Chernyshev, 2017; Dubinina et al., 2010; 2014; Tarasova et al., 2020). This indicates that the granitoid magmatism served only as a source of heat for the ore-forming systems. In turn, the close spatial relationships between the early veinlet-disseminated sulfide ores and quartz veins observed in many deposits, such as Sukhoi Log, as well as the similarity of their isotopic characteristics, suggest the possibility of reworking the early ores by the fluid which then formed the late quartz veins.

7. Conclusions

This study provides new geochronological data for four Sukhoi Log-type orogenic deposits located in the world-class Bodaibo District (Northern Transbaikalia) gold-mining subprovince of the Baikal-Patom Belt. The combination of the Rb-Sr and ^{40}Ar-^{39}Ar isotope data allowed us to propose the existence of two ore-forming events in the region. The earliest event that occurred in the Silurian period (450–430 Ma) resulted in the formation of the gold-bearing veinlet-disseminated sulfide ores, which are of main economic significance for the region. The rejuvenation of the ore-forming processes in the region took placed during the Middle Carboniferous (340–330 Ma) and was associated with the formation of the large-scale granitoid intrusions. This later event likely caused the disturbance of the U-Th-Pb isotopic system in the hydrothermal monazite from the early ores, which led to discordant U-Pb data (Yudovskaya et al., 2011). The results of this study support the genetic model for the Sukhoi Log-type deposits whereby the early veinlet-disseminated sulfide ores were formed via the circulation of metamorphic metal-bearing fluids sourced from the Neoproterozoic sedimentary sequences of the BPB.

It is important to note that orogenic gold deposits with similar Early Carboniferous (370–360 Ma) ages are also known in the East Sayan gold province located west of the BPB (Damdinov et al., 2018). An Early Paleozoic (480–450 Ma) magmatic event, which was the cause of the intrusion-related formation of the gold deposits, has also been established in the region (Damdinov et al., 2021). By contrast, the Baikal-Muya gold province located south of the BPB hosts only younger (Early Permian) orogenic deposits (Chugaev et al., 2020 and references therein).

Declaration of Competing Interest

The authors declare that they have no known competing financial interests or personal relationships that could have appeared to influence the work reported in this paper.

Acknowledgements

Constructive and thorough reviews by Sebastien Meffre and two anonymous reviewers are gratefully acknowledged. This study was financially supported by the project of the Russian Federation represented by the Ministry of Science and Higher Education of the Russian Federation (grant № 13.1902.21.008, agreement 075-15-2020-802). The authors are grateful to Olga Plotinskaya and Konstantin Shatagin (IGEM RAS) for comments and suggestions which helped improve the manuscript.

Appendix A. Supplementary data

Supplementary data to this article can be found online at https://doi.org/10.1016/j.oregeorev.2022.104855.

References

Babyak, V., Blinov, A., Tarasova, J., Budyak, A., 2019. New data on the geological and structural features of the Ozhereliye, Ykanskoye, Ugahan and Golets Vysochaishy gold fields. Earth Sci. Subsoil Use 42 (4), 388–412.

Baksi, A.K., 1999. Reevaluation of plate motion models based on hotspot tracks in the Atlantic and Indian Oceans. J. Geol. 107, 13–26. https://doi.org/10.1086/314329.

Baksi, A.K., 2006. Guidelines for assessing the reliability of $^{40}Ar/^{39}Ar$ plateau ages: application to ages relevant to hotspot tracks. http://www.mantleplumes.org/ArAr.html (accessed October 2021).

Baksi, A.K., Archibald, D.A., Farrar, E., 1996. Intercalibration of ^{40}Ar–^{39}Ar dating standards. Chem. Geol. 129, 307–324. https://doi.org/10.1016/0009-2541(95)00154-9.

Belogub, E.V., Palenova, E.E., Chugaev, A.V., Plotinskaya, O.Y., 2014. Origin of gold ores in black-shale hosted deposits of the Bodaybo region, Russia. Acta Geol. Sinica 88, 252–253. https://doi.org/10.1111/1755-6724.12370_2.

Bettinelli, M., Beone, G.M., Spezia, S., Baffi, C., 2000. Determination of heavy metals in soils and sediments by microwave-assisted digestion and inductively coupled plasma optical emission spectrometry analysis. Anal. Chim. Acta 424, 289–296. https://doi.org/10.1016/S0003-2670(00)01123-5.

Bogdanova, S.V., Pisarevskii, S.A., Li, Z.X., 2009. Assembly and breakup of Rodinia (some results of IGCP Project 440). Stratigr. Geol. Correl. 17, 259–274. https://doi.org/10.1134/S0869593809030022.

Budyak, A.E., Goryachev, N.A., Skuzovatov, S.Y., 2016. Geodynamic background for large-scale mineralization in the southern environs of the Siberian Craton in the Proterozoic. Dokl. Earth Sci. 470, 1063–1066. https://doi.org/10.1134/S1028334X1610010X.

Budyak, A.E., Skuzovatov, S.Y., Tarasova, Y.I., Goryachev, N.A., Wang, K.L., 2019. Common Neoproterozoic-Early Paleozoic evolution of ore-bearing sedimentary complexes in the southern Siberian Craton. Dokl. Earth Sci. 484, 92–96. https://doi.org/10.1134/S1028334X19010227.

Buryak, V.A., 1982. Metamorphism and Ore Formation. Moscow: Nedra. 256. (in Russian).

Buryak, V.A., Bakulin, Yu.I., 1998. Metallogeny of gold. Vladivostok: Dal'nauka. 403. (in Russian).

Buryak, V.A., Goncharov, V.I., Goryachev, N.A., 2002. Evolutionary series of large deposits of gold and platinum group metals in carbonaceous sequences. Dokl. Earth Sci. 387, 1007–1009.

Buryak, V.A., Khmelevskaya, N.M., 1997. Sukhoi Log – One of the largest gold deposits in the world (genesis, patterns of mineralization distribution, forecasting criteria). Vladivostok: Dal'nauka. 157. (in Russian).

Chernyshev, I.V., Bortnikov, N.S., Chugaev, A.V., Gamyanin, G.N., Bakharev, A.G., 2011. Metal sources of the large Nezhdaninsky orogenic gold deposit, Yakutia, Russia: results of high-precision MC-ICP-MS analysis of lead isotopic composition supplemented by data on strontium isotopes. Geol. Ore Deposits 53, 353–373. https://doi.org/10.1134/S1075701511050035.

Chernyshev, I.V., Chugaev, A.V., Safonov, Y.G., Saroyan, M.R., Yudovskaya, M.A., Eremina, A.V., 2009. Lead isotopic composition from data of high-precession MC-ICP-MS and sources of matter in the large-scale Sukhoi Log noble metal deposit, Russia. Geol. Ore Deposits 51, 496–504. https://doi.org/10.1134/S1075701509060063.

Chugaev, A.V., Chernyshev, I.V., 2017. Pb–Pb isotopic systematics of orogenic gold deposits of the Baikal-Patom fold belt (Northern Transbaikalia, Russia) and estimation of the role of Neoproterozoic crust in their formation. Geochem. Int. 55, 1010–1021. https://doi.org/10.1134/S0016702917110040.

Chugaev, A.V., Chernyshev, I.V., Dubinina, E.O., Shatagin, K.N., Budyak, A.E., Tarasova, Y.I., Skuzovatov, S.Y., Gareev, B.I., Goryachev, N.A., 2018. Isotopic (Sm–Nd, Pb–Pb, and $\delta^{34}S$) and geochemical characteristics of the metasedimentary rocks of the Baikal-Patom belt (Northern Transbaikalia) and Evolution of the Sedimentary Basin in the Neoproterozoic. Petrology 26, 213–245. https://doi.org/10.1134/S0869591118030025.

Chugaev, A.V., Chernyshev, I.V., Gamyanin, G.N., Bortnikov, N.S., Baranova, A.N., 2010. Rb-Sr isotopic systematic of hydrothermal minerals, age, and matter sources of the Nezhdaninskoe gold deposit (Yakutia). Dokl. Earth Sci. 434 (2), 1337–1341. https://doi.org/10.1134/S1028334X10100107.

Chugaev, A.V., Chernyshev, I.V., Shatagin, K.N., Oleinikova, T.I., Budyak, A.E., Tarasova, Y.I., Skuzovatov, S.Y., 2017. Sources of clastic material of the Neoproterozoic metasedimentary rocks of the Baikal-Patom belt, Northern Transbaikalia: Evidence from Sm-Nd isotope data. Geochem. Int. 55, 60–68. https://doi.org/10.1134/S0016702916120028.

Chugaev, A.V., Dubinina, E.O., Chernyshev, I.V., Travin, A.V., Kossova, S.A., Larionova, Y.O., Nosova, A.A., Plotinskaya, O.Y., Oleinikova, T.I., Sadasyuk, A.S., 2020. Sources and age of the gold mineralization of the Irokinda deposit, Northern Transbaikalia: evidence from Pb, S, Sr, and Nd isotope-geochemical and ^{39}Ar–^{40}Ar geochronological data. Geochem. Int. 58, 1208–1227. https://doi.org/10.1134/S0016702920110051.

Chugaev, A.V., Plotinskaya, O.Y., Chernyshev, I.V., Kotov, A.A., 2014. Lead isotope heterogeneity in sulfides from different assemblages at the Verninskoe gold deposit (Baikal-Patom Highland, Russia). Dokl. Earth Sci. 457, 887–892. https://doi.org/10.1134/S1028334X14070216.

Chumakov, N.M., 2016. Early Vendian stage of folding in the Patom folded zone: Syn-folded clastic dikes in the Dalnetaiginsky group, Central Siberia. Stratigr. Geol. Correl. 24, 212–217. https://doi.org/10.1134/S0869593816020027.

Chumakov, N.M., Semikhatov, M.A., Sergeev, V.N., 2013. Vendian reference section of southern middle Siberia. Stratigr. Geol. Correl. 21, 359–382. https://doi.org/10.1134/S0869593813040023.

Cliff, R.A., 1985. Isotopic dating in metamorphic belts. J. Geol. Soc. Lond. 142, 97–110. https://doi.org/10.1144/gsjgs.142.1.0097.

Damdinov, B.B., Huang, X.W., Goryachev, N.A., Zhmodik, S.M., Mironov, A.G., Damdinova, L.B., Khubanov, V.B., Reutsky, V.N., Yudin, D.S., Travin, A.V., Posokhov, V.F., 2021. Intrusion-hosted gold deposits of the southeastern East Sayan (northern Central Asian Orogenic Belt, Russia). Ore Geol. Rev. 139, 104541 https://doi.org/10.1016/j.oregeorev.2021.104541.

Damdinov, B.B., Zhmodik, S.M., Travin, A.V., Yudin, D.S., Goryachev, N.A., 2018. New data on the age of gold mineralization in the southeastern part of Eastern Sayan. Dokl. Earth Sc. 479, 429–432. https://doi.org/10.1134/S1028334X18040116.

De Boorder, H., 2012. Spatial and temporal distribution of the orogenic gold deposits in the Late Palaeozoic Variscides and Southern Tianshand. How orogenic are they? Ore Geol. Rev. 46, 1–31. https://doi.org/10.1016/j.oregeorev.2012.01.002.

Distler, V.V., Yudovskaya, M.A., Prokof'ev, V.Y., Lishnevskii, E.N., Mitrofanov, G.L., 2004. Geology, composition and genesis on the Sukhoi Log noble metals deposit, Russia. Ore Geol. Rev. 24, 7–44. https://doi.org/10.1016/j.oregeorev.2003.08.007.

Dodson, M.H., 1979. In: Lectures in Isotope Geology. Springer-Vergal, New-York, pp. 194–202.

Donskaya, T.V., Gladkochub, D.P., Mazukabzov, A.M., Ivanov, A.V., 2013. Late Paleozoic-Mesozoic subduction-related magmatism at the southern margin of the Siberian continent and the 150 million-year history of the Mongol-Okhotsk Ocean. J. Asian Earth Sci. 62, 79–97. https://doi.org/10.1016/j.jseaes.2012.07.023.

Dubinina, E.O., Chugaev, A.V., Ikonnikova, T.A., Avdeenko, A.S., Yakushev, A.I., 2014. Sources and fluid regime of quartz–carbonate veins at the Sukhoi Log gold deposit, Baikal-Patom Highland. Petrology 22, 329–358. https://doi.org/10.1134/S0869591114040031.

Dubinina, E.O., Ikonnikova, T.A., Chugaev, A.V., 2010. Heterogeneity of the sulfur isotopic composition of pyrite at the Sukhoi Log deposit and Its controlling factors. Dokl. Earth Sci. 435, 1665–1669. https://doi.org/10.1134/S1028334X1012024X.

Faure, G., 1986. Principles of Isotope Geology. New York, Chichester, Brisbane, Toronto, Singapor:Wiley, 589. 10.1017/S0016756800017453.

Fleck, R.J., Sutter, J.F., Elliot, D.H., 1977. Interpretation of discordant 40Ar/39Ar age spectra of Mesozoic tholeiites from Antarctica. Geochim. Cosmochim. Acta 41, 15–32. https://doi.org/10.1016/0016-7037(77)90184-3.

Frei, R., Dahl, P.S., Frandsson, M.M., Jensen, L.A., Hansen, T.R., Terry, M.P., Frei, K.M., 2009. Lead-isotope and trace-element geochemistry of Paleoproterozoic metasedimentary rocks in the Lead and Rochford basins (Black Hills, South Dakota, USA): implications for genetic models, mineralization ages, and sources of leads in the Homestake gold deposit. Precambr. Res. 172, 1–24. https://doi.org/10.1016/j.precamres.2009.03.004.

Gladkochub, D.P., Stanevich, A.M., Mazukabzov, A.M., Donskaya, T.V., Motova, Z.L., Kornilova, T.A., Pisarevsky, S.A., Nicoll, G., 2013. Early evolution of the Paleoasian ocean: LA-ICP-MS dating of detrital zircon from Late Precambrian sequences of the southern margin of the Siberian craton. Russ. Geol. Geophys. 54, 1150–1163. https://doi.org/10.1016/j.rgg.2013.09.002.

Goldfarb, R.J., Baker, T., Dubé, B., Groves, D.I., Hart, C.J., Gosselin, P., 2005. Distribution, character, and genesis of gold deposits in metamorphic Terranes. Econ. Geol. 100, 407–450. https://doi.org/10.5382/AV100.14.

Goldfarb, R.J., Taylor, R.D., Collins, G.S., Goryachev, N.A., Orlandini, O.F., 2014. Phanerozoic continental growth and gold metallogeny of Asia. Gondwana Res. 25, 48–102. https://doi.org/10.1016/j.gr.2013.03.002.

Goldfarb, R.J., Groves, D.I., 2015. Orogenic gold: common or evolving fluid and metal sources through time. Lithos 233, 2–26. https://doi.org/10.1016/j.lithos.2015.07.011.

Goldfarb, R.J., Groves, D.I., Gardoll, S., 2001. Orogenic gold and geologic time: a global synthesis. Ore Geol. Rev. 18, 1–75. https://doi.org/10.1016/S0169-1368(01)00016-6.

Groves, D.I., 1993. The crustal continuum model for late-Archaean lode gold deposits of the Yilgarn block, Western Australia. Miner. Depos. 28, 366–374. https://doi.org/10.1007/BF02431596.

Groves, D.I., Goldfarb, R.J., Gebre-Mariam, M., Hagemann, S.G., Robert, F., 1998. Orogenic gold deposits: a proposed classification in the context of their crustal distribution and relationship to other gold deposit types. Ore Geol. Rev. 13, 7–27. https://doi.org/10.1016/S0169-1368(97)00012-7.

Groves, D.I., Hart, C.J.R., Goldfarb, R.J., Robert, F., 2003. Gold deposits in metamorphic belts: overview of current understanding, outstanding problems, future research, and exploration significance. Econ. Geol. 98, 1–29. https://doi.org/10.2113/gsecongeo.98.1.1.

Groves, D.I., Santosh, M., 2016. The giant Jiaodong gold province: the key to a unified model for orogenic gold deposits? Geosci. Front. 7, 409–417. https://doi.org/10.1016/j.gsf.2015.08.002.

Gusev, G.S., Khain, V.E., 1995. On relations between Baikal-Vitim, Aldan-Stanovoi and Mongol-Okhotsk terranes (south of Mid-Siberia). Geotectonics 5, 68–82 in Russian.

Hess, J.C., Lippolt, H.J., Wirth, R., 1987. Interpretation of ^{40}Ar/^{39}Ar spectra of biotites: evidence from hydrothermal degassing experiments and TEM studies. Chem. Geol. 66, 137–149. https://doi.org/10.1016/0168-9622(87)90036-4.

Ivanov, A.I., 2008. The Ozherelie deposit is new type gold mineralization in Bodaibo gold-mining region. Proc. Siberian Branch Acad. Earth Sci. Russ. Acad. Nat. Sci. 6, 14–26 in Russian.

Ivanov, A.I., 2014. Gold of Baikal-Patom (Geology, Mineralization, and Prospects). Central Research Institute of Geological Prospecting for Basic and Precious Metals, Moscow, 215. (in Russian).

Ivanov, A.I., Livshits, V.I., Perevalov, O.V., et al., 1995. Dokembrii Patomskogo Highlands (Precambrian of the Patom Highland), Moscow: Nedra. 352. (in Russian).

Ivanov, A.V., Vanin, V.A., Demonterova, E.I., Gladkochub, D.P., Donskaya, T.V., Gorovoy, V.A., 2015. Application of the 'no fool's clock'to dating the Mukodek gold field, Siberia, Russia. Ore Geol. Rev. 69, 352–359. https://doi.org/10.1016/j.oregeorev.2015.03.007.

Iwata, N., Kaneoka, I., 2000. On the relationships between the ^{40}Ar-^{39}Ar dating results and the conditions of basaltic samples. Geochem. J. 34, 271–281. https://doi.org/10.2343/geochemj.34.271.

Karpenko, I.A., Migachev, I.F., Mikhailov, B.K., Petrash, N.G., 2006. Current geological and economic estimation of the Sukhoi Log deposit. Rudy Met. 2, 22–27.

Kelley, S., 2002. Excess argon in K-Ar and Ar-Ar geochronology. Chem. Geol. 188, 1–22. https://doi.org/10.1016/S0009-2541(02)00064-5.

Kendrick, M.A., Burgess, R., Pattrick, R.A.D., Turner, P.G., 2001. Halogen and Ar-Ar age determinations of inclusions within quartz veins from porphyry copper deposits using complementary noble gas extraction techniques. Chem. Geol. 177, 351–370. https://doi.org/10.1016/S0009-2541(00)00419-8.

Kerrich, R., Cassidy, K.F., 1994. Temporal relationships of lode-gold mineralization to accretion, magmatism, metamorphism, and deformation – Archean to present: a review. Ore Geol. Rev. 9, 263–310. https://doi.org/10.1016/0169-1368(94)90001-9.

Konstantinov, M.M., 2010. The Lena Gold Ore Province. In: Konstantinov, M.M. (Ed.), Gold deposits of Russia. Aquarely Inc., Moscow, pp. 15–31 in Russian.

Korikovsky, S.P., Fedorovsky, V.S., 1980. Early Precambrian of the Patom Upland. Moscow. Science 300 in Russian.

Kostitsyn, Y.A., 1989. Processing of isochrones in the presence of geochemical dispersion. Geochem. Int. 5, 632 in Russian.

Kröner, A., Kovach, V., Rytsk, E., Belousova, E., Hegner, E., Armstrong, R., Dolgopolova, A., Seltmann, R., Alexeiev, D.V., Degtyarev, K.E., Hoffmann, J.E., Wong, J., Sun, M., Cai, K., Wang, T., Tong, Y., Wilde, S.A., 2014. Reassessment of continental growth during the accretionary history of the Central Asian orogenic belt. Gondwana Res. 25, 103–125. https://doi.org/10.1016/j.gr.2012.12.023.

Kuz'min, M.I., Spiridonov, A.I., Nemerov, V.K., Yarmolyuk, V.V., Ivanov, A.I., Mitrofanov, G.L., 2006. Geodynamic setting of gold ore deposits of the Neoproterozoic Bodaibo trough. Dokl. Earth Sci. 407, 397–400. https://doi.org/10.1134/S1028334X06030123.

Lanphere, M.A., Dalrymple, G.B., 1976. Identification of excess ^{40}Ar by the ^{40}Ar/^{39}Ar age spectrum technique. Earth Planet. Sci. Lett. 32, 141–148. https://doi.org/10.1016/0012-821X(76)90052-2.

Large, R.R., Bull, S.W., Maslennikov, V.V., 2011. A carbonaceous sedimentary source rock model for Carlin-type and orogenic gold deposits. Econ. Geol. 106, 331–358. https://doi.org/10.2113/econgeo.106.3.331.

Large, R.R., Danyushevsky, L.V., Chang, Z., Maslennikov, V.V., Robert, F., 2007. Multistage sedimentary and methamorphic origin of pyrite and gold in the giant Sukhoi Log deposit, Lena gold province, Russia. Econ. Geol. 102, 1233–1267. https://doi.org/10.2113/gsecongeo.102.7.1233.

Larionova, Y.O., Samsonov, A.V., Shatagin, K.N., Nosova, A.A., 2013. Isotopic geochronological evidence for the Paleoproterozoic age of gold mineralization in Archean greenstone belts of Karelia, the Baltic Shield. Geol. Ore Deposits 55, 320–340. https://doi.org/10.7868/S0016777013050055.

Laverov, N.P., Lishnevskii, E.N., Distler, V.V., Chernov, A.A., 2000. Model of the ore-magmatic system of the Sukhoi Log gold-platinum deposit, Eastern Siberia. Russia. Dokl. Earth Sci. 375, 1362–1365.

Laverov, N.P., Chernyshev, I.V., Chugaev, A.V., Bairova, E.D., Gol'tsman, Y.V., Distler, V. V., Yudovskaya, M.A., 2007. Formation stages of the large-scale noble metal mineralization in the Sukhoi Log deposit, east Siberia: results of isotope-geochronological study. Dokl. Earth Sci. 415, 810–814. https://doi.org/10.1134/S1028334X07050339.

Ludwig, K.R., 2009. Isoplot/Ex ver 3.71: A geochronological toolkit for Microsoft Excel. Berkeley Geochronology Center Special Publication 4, 77.

L'vova, N.A., 1969. To the study of the stratification of the Bodaibo sub-series. Questions of geology and gold content of the Lensky region. Irkutsk 11–77 in Russian.

Mao, J., Wang, Y., Li, H., Pirajno, F., Zhang, C.h., Wang, R., 2008. The relationship of mantle-derived fluids to gold metallogenesis in the Jiaodong Peninsula: evidence from D-O–C–S isotope systematics. Ore Geol. Rev. 33, 361–381. https://doi.org/10.1016/j.oregeorev.2007.01.003.

Meffre, S., Large, R.R., Scott, R., Chang, Z., Gilbert, S.E., Danyushevsky, L.V., Woodhead, J., Hergt, J.M., Maslennikov, V., 2008. Age and pyrite Pb-isotopic

composition of the giant Sukhoi Log sediment-hosted gold deposit, Russia. Geochim. Cosmochim. Acta 72, 2377–2391. https://doi.org/10.1016/j.gca.2008.03.005.
Meffre, S., Large, R.R., Steadman, J.A., Gregory, D.D., Stepanov, A.S., Kamenetsky, V.S., Kathy Ehrig, K., Scott, R.J., 2016. Multi-stage enrichment processes for large gold-bearing ore deposits. Ore Geol. Rev. 76, 268–279. https://doi.org/10.1016/j.oregeorev.2015.09.002.
Nemerov, V.K., Razvozzhaeva, E.A., Budyak, A.E., Stanevich, A.M., Kornilova, T.A., 2010. Biogenic sedimentation factors of mineralization in the Neoproterozoic strata of the Baikal-Patom region. Russ. Geol. Geophys. 51, 572–586. https://doi.org/10.1016/j.rgg.2010.04.012.
Neymark, L.A., Rytsk, E.Y., Rizvanova, N.G., 1993. The Hercynian age and Precambrian crustal protolith of the Barguzin granitoids of the Angara-Vitim batholith: U-Pb and Sm–Nd isotope evidence. Proc. Acad. Sci. 331, 726–729 in Russian.
Novikova, S., Sokol, E., Khvorov, P., 2016. Multiple combustion metamorphic events in the Goose Lake Coal Basin, Transbaikalia, Russia: first dating results. Quat. Geochronol. 36, 38–54. https://doi.org/10.1016/j.quageo.2016.08.001.
Onstott, T.C., Miller, M.L., Ewing, R.C., Arnold, G.W., Walsh, D.S., 1995. Recoil refinements: implications for the $^{40}Ar/^{39}Ar$ dating technique. Geochim. Cosmochim. Acta 59, 1821–1834. https://doi.org/10.1016/0016-7037(95)00085-E.
Palenova, E.E., Belogub, E.V., Novoselov, K.A., Maslennikov, V.V., Kotlyarov, V.A., Blinov, I.A., Plotinskaya, O.Y., Griboedova, I.G., Kuzmenko, A.A., 2015. Chemical evolution of pyrite at the Kopylovsky and Kavkaz black shale-hosted gold deposits, Bodaybo district, Russia: evidence from EPMA and LA-ISP-ms data. Geol. Ore Deposits 57, 64–84. https://doi.org/10.1134/S107570151501002X.
Phillips, G.N., 2013. Australian and global setting for gold in 2013, in Proceedings world gold 2013, Brisbane, Australia, 26–29 September. Aust. Inst. Min. Metall. 15–21.
Pokrovsky, B.G., Bujakaite, M.I., 2015. Geochemistry of C, O, and Sr isotopes in the Neoproterozoic carbonates from the southwestern Patom paleobasin, southern Middle Siberia. Lithol. Miner. Resour. 50, 144–169. https://doi.org/10.1134/S0024490215010046.
Pokrovsky, B.G., Bujakaite, M.I., Melezhik, V.A., 2006. Carbon, oxygen, strontium, and sulfur isotopic compositions in late Precambrian rocks of the Patom Complex, central Siberia: communication 1. Results, isotope stratigraphy, and dating problems. Lithol. Miner. Resour. 41, 450–474. https://doi.org/10.1134/S0024490206050063.
Pokrovsky, B.G., Chumakov, N.M., Bujakaite, M.I., Melezhik, V.A., 2010. Geochemical properties of Neoproterozoic "Cap Dolomites" in the patom paleobasin and problem of their genesis. Lithol. Miner. Resour. 45, 577–592. https://doi.org/10.1134/S0024490210060052.
Powerman, V., Shatsillo, A., Chumakov, N., Kapitonov, I., Hourigan, J., 2015. Interaction between the Central Asian Orogenic Belt (CAOB) and the Siberian Craton as recorded by detrital zircon suites from Transbaikalia. Precambr. Res. 267, 39–71. https://doi.org/10.1016/j.precamres.2015.05.015.
Prokof'ev, V.Y., Safonov, Y.G., Lüders, V., Borovikov, A.A., Kotov, A.A., Zlobina, T.M., Murashov, K.Y., Yudovskaya, M.A., Selektor, S.L., 2019. The sources of mineralizing fluids of orogenic gold deposits of the Baikal-Patom and Muya areas, Siberia: constraints from the C and N stable isotope compositions of fluid inclusions. Ore Geol. Rev. 111, 102988.
Qiu, H.-N., Zhu, B.-Q., Sun, D., 2002. Age significance interpreted from 40Ar-39Ar dating of quartz samples from the Dongchuan Copper Deposits, Yunnan, SW China, by crushing and heating. Geochem. J. 36, 475–491. https://doi.org/10.2343/geochemj.36.475.
Ruffet, G., Innocent, C., Michard, A., Féraud, G., Beauvais, A., Nahon, D., Hamelin, B., 1996. A geochronological ^{40}Ar-^{39}Ar and ^{87}Rb-^{86}Sr study of K-Mn oxides from the weathering sequence of Azul, Brazil. Geochim. Cosmochim. Acta 60, 2219–2232. https://doi.org/10.1016/0016-7037(96)00080-4.
Rundqvist, I.K., Bobrov, V.A., Smirnova, T.N., 1992. Formation stages of the bodaibo gold region. Geol. Ore Deposits 34, 3–15. In Russian.
Rusinov, V.L., Borisovsky, S.E., Rusinova, O.V., Kryazhev, S.G., Shchegol'kov, Y.V., Alysheva, E.I., 2008. Wall-rock metasomatism of carbonaceous terrigenous rocks in the Lena gold district. Geol. Ore Deposits 50, 1–40. https://doi.org/10.1134/S1075701508010017.
Safonov, Yu.G., Prokofiev, V.Yu., Kotov, AA, Saroyan, M.R., 2012. P-T parameters of ore-forming fluids as indicators of geotectonic settings for the formation of gold deposits in the Baikal-Patom Highlands. Proceedings of XV All-Russian Conference on Thermobarogeochemistry. Moscow. Russia. 75–77. (in Russian).
Safonova, I.Y., Kotlyarov, A., Krivonogov, S., 2017. Intra-oceanic arcs of the Paleo-Asian ocean. Geodyn. Tectonophys. 8, 547–550. https://doi.org/10.5800/GT-2017-8-3-0287.
Scott, R.J., Large, R.R., Meffre, S., Maslennikov, V.V., 2007. Structural controls on the development of the giant Sukhoi Log gold deposit, Siberia: Deformation in the desert. In Geological Society of Australia Specialist Group in Tectonics and Structural Geology Alice Springs, 55.
Steiger, R.H., Jäger, E., 1977. Subcommission on geochronology: convention on the use of decay constants in geo- and cosmochronology. Earth Planet. Sci. Lett. 36, 359–362. https://doi.org/10.1016/0012-821X(77)90060-7.
Szczerba, M., Derkowski, A., Kalinichev, A.G., Srodon, J., 2015. Molecular modeling of the effects of ^{40}Ar recoil in illite particles on their K-Ar isotope dating. Geochim. Cosmochim. Acta 159, 162–176. https://doi.org/10.1016/j.gca.2015.03.005.
Tarasova, Y.I., Budyak, A.E., Chugaev, A.V., Goryachev, N.A., Tauson, V.L., Skuzovatov, S.Y., Bryukhanova, N.N., Parshin, A.V., Abramova, V.D., Gareev, B.I., Reutsky, V.N., 2020. Mineralogical and isotope-geochemical ($\delta^{13}C$, $\delta^{34}S$ and Pb-Pb) characteristics of the Krasniy gold mine (Baikal-Patom Highlands): constraining ore-forming mechanisms and the model for Sukhoi Log-type deposits. Ore Geol. Rev. 119, 103365 https://doi.org/10.1016/j.oregeorev.2020.103365.
Tarasova, Yu.I., Budyak, A.E., Ivanov, A.V., Goryachev, N.A., Ignatiev, A.V., Radomskaya, T.A., Velivetskaya, T.A., Radomskaya, T.A., Blinov, A.V., Babiak, V.N., 2021. Typomorphism, typochemistry, and isotopic characteristics of pyrite from the Golets Vysokiy deposit (Eastern Siberia). Geol. Ore Deposits CI, 63–75. 10.31857/S0869605521010123. (in Russian).
Tauson, V.L., Akimov, V.V., Lipko, S.V., Spiridonov, A.M., Budyak, A.E., Belozerova, O. Y., Smagunov, N.V., 2015. Typomorphism of pyrite of the Sukhoi Log deposit (East Siberia). Russ. Geol. Geophys. 56 (10), 1394–1413. https://doi.org/10.1016/j.rgg.2015.09.003. (in Russian).
Thirlwall, M.F., 1991. Long-term reproducibility of multicollector Sr and Nd isotope ratio analysis. Chem. Geol.: Isotope Geosci. Sect. 94 (2), 85–104. https://doi.org/10.1016/S0009-2541(10)80021-X.
Travin, A.V., Yudin, D.S., Vladimirov, A.G., Khromykh, S.V., Volkova, N.I., Mekhonoshin, A.S., Kolotilina, T.B., 2009. Thermochronology of the Chernorud granulite zone, Ol'khon Region, Western Baikal area. Geochem. Int. 47, 1107–1124. https://doi.org/10.1134/S0016702909110068.
Tsygankov, A.A., Burmakina, G.N., Khubanov, V.B., Buyantuev, M.D., 2017. Geodynamics of Late Paleozoic batholith-forming processes in western Transbaikalia. Petrology 25, 396–418. https://doi.org/10.1134/S0869591117030043.
Tsygankov, A.A., Litvinovsky, B.A., Jahn, B.M., Reichow, M.K., Liu, D.Y., Larionov, A.N., Presnyakov, S.L., Lepekhina, Y.N., Sergeev, S.A., 2010. Sequence of magmatic events in the Late Paleozoic of Transbaikalia, Russia (U–Pb isotope data). Russ. Geol. Geophys. 51 (9), 972–994.
Villa, I.M., 1997. Direct determination of ^{39}Ar recoil distance. Geochim. Cosmochim. Acta 61, 689–691. https://doi.org/10.1016/S0016-7037(97)00002-1.
Villa, I.M., 2021. The in vacuo release of Ar from minerals: 1. Hydrous minerals. Chem. Geol. 564, 120076 https://doi.org/10.1016/j.chemgeo.2021.120076.
Villa, I.M., De Bièvre, P., Holden, N.E., Renne, P.R., 2015. IUPAC-IUGS recommendation on the half life of ^{87}Rb. Geochim. Cosmochim. Acta 164, 382–385. https://doi.org/10.1016/j.gca.2015.05.025.
Villa, I.M., Grobety, B., Kelley, S.P., Trigila, R., Wieler, R., 1996. Assessing Ar transport paths and mechanisms for McClure Mountains Hornblende. Contrib. Mineral. Petrol. 126, 67–80. https://doi.org/10.1007/s004100050236.
Vinogradov, V.I., Pichugin, L.P., Bykhover, V.N., Golovin, D.I., Muravyev, V.I., Buyakaite, M.I., 1996. Isotopic features and time of epigenetic transformations of the Upper Precambrian deposits of the Ura uplift. Lithol. Miner. Resour. 1, 68–78 in Russian.
White, L.T., Ireland, T.R., 2012. High-uranium matrix effect in zircon and its implications for SHRIMP U-Pb age determinations. Chem. Geol. 306, 78–91. https://doi.org/10.1016/j.chemgeo.2012.02.025.
Wijbrans, J.R., McDougall, I., 1986. $^{40}Ar/^{39}Ar$ dating of white micas from an Alpine high-pressure metamorphic belt on Naxos (Greece): the resetting of the argon isotopic system. Contrib. Miner. Petrol. 93 (2), 187–194.
Wood, B.L., Popov, N.P., 2006. The giant Sukhoi Log gold deposit (Siberia). Russ. Geol. Geophys. 47, 315–341.
Yakubchuk, A., Stein, H., Wilde, A., 2014. Results of pilot Re–Os dating of sulfides from the Sukhoi Log and Olympiada orogenic gold deposits, Russia. Ore Geol. Rev. 59, 21–28. https://doi.org/10.1016/j.oregeorev.2013.12.003.
Yarmolyuk, V.V., Kozlovsky, A.M., Kovach, V.P., Kozakov, I.K., Kotov, A.B., Rytsk, E.Y., 2012. Mechanisms of continental crust formation in the Central Asian foldbelt. Geotectonics 46, 251–272. https://doi.org/10.1134/S001685211204005X.
York, D., 1966. Least-squares fitting of a straight line. Can. J. Phys. 44, 1079–1086. https://doi.org/10.1139/P66-090.
Yudin, D., Murzintsev, N., Travin, A., Alifirova, T., Zhimulev, E., Novikova, S., 2021. Studying the stability of the K/Ar isotopic system of phlogopites in conditions of high T, P: $^{40}Ar/^{39}Ar$ dating, laboratory experiment, numerical simulation. Minerals 11, 192. https://doi.org/10.3390/min11020192.
Yudovskaya, M.A., Distler, V.V., Mokhov, A.V., Rodionov, N.V., Antonov, A.V., Sergeev, S.A., 2011. Relationship between metamorphism and ore formation at the Sukhoi Log gold deposit hosted in black slates from the data of U-Th-Pb isotopic SHRIMP-dating of accessory minerals. Geol. Ore Deposits 53, 27–57. https://doi.org/10.1134/S1075701511010077.
Yudovskaya, M.A., Distler, V.V., Prokof'ev, V.Y., Akinfiev, N.N.,, 2016. Gold mineralization and orogenic metamorphism in the Lena Province of Siberia as assessed from Chertovo Koryto and Sukhoi Log deposits. Geochem. Front. 7, 453–481. https://doi.org/10.1016/j.gsf.2015.07.010.
Zhai, D., Liu, J., Ripley, E.M., Wang, J., 2015. Geochronological and He–Ar–S isotopic constraints on the origin of the Sandaowanzi gold-telluride deposit, northeastern China. Lithos 212, 338–352. https://doi.org/10.1016/j.lithos.2014.11.017.
Zhuravleva, Z.A., Komar, V.A., Chumakov, N.M., 1969. Structure and correlation of the Upper Precambrian deposits of western Yakutia. Proceedings interdepartmental meeting on the development of unified stratigraphic schemes of the Yakut ASSR. Mater. Geol. Minerals YaSSR 13, 53–69 in Russian.
Zonenshain, L.P., Kuzmin, M.I., Natapov, L.M., 1990. Geology of the USSR: A plate tectonic synthesis. Am. Geophys. Union, Geodyn. Ser. 21, 242. https://doi.org/10.1029/GD021.
Zongyong, W., Xin, H., Guxian, L.V., Xunyu, Z., Yingchun, Z., Xiao, F., Qinglong, H., Yaqing, X., 2016. Rb-Sr Isotopic geochronology and geological implications of Dongfeng gold deposit in Jiaodong area. Earth Sci. Res. J. 20, 11–17. https://doi.org/10.15446/esrj.v20n1.55178.
Zorin, Y.A., Mazukabzov, A.M., Gladkochub, D.P., Donskaya, T.V., Presnyakov, S.L., Sergeev, S.A., 2008. Silurian age of major folding in the Riphaean deposits of the Baikal-Patom zone. Dokl. Earth Sci. 423, 1235–1239. https://doi.org/10.1134/S1028334X08080114.